



**HAL**  
open science

# Topological photonics in polariton lattices

Alberto Amo

► **To cite this version:**

Alberto Amo. Topological photonics in polariton lattices. Optics [physics.optics]. Université de Lille, 2022. tel-03854616

**HAL Id: tel-03854616**

**<https://theses.hal.science/tel-03854616>**

Submitted on 15 Nov 2022

**HAL** is a multi-disciplinary open access archive for the deposit and dissemination of scientific research documents, whether they are published or not. The documents may come from teaching and research institutions in France or abroad, or from public or private research centers.

L'archive ouverte pluridisciplinaire **HAL**, est destinée au dépôt et à la diffusion de documents scientifiques de niveau recherche, publiés ou non, émanant des établissements d'enseignement et de recherche français ou étrangers, des laboratoires publics ou privés.

# Topological photonics in polariton lattices



**Alberto Amo**

Laboratoire de Physique des Lasers, Atomes et Molécules  
Université de Lille - CNRS

Mémoire présentée en vue de l'obtention de  
l'habilitation à diriger des recherches

Membres du jury:

- Pr. Marc Lefranc, Université de Lille (rapporteur)
- Pr. Fabrice Mortessagne, Université Côte d'Azur (rapporteur)
- Pr. Henning Shommerus, University of Lancaster (rapporteur)
- Pr. Dr. Cristiane Morais Smith, University of Utrecht (examinatrice)
- Pr. Pierre Suret, Université de Lille (examineur, garant)

19 octobre 2022



# Contents

<b>Foreword</b>	<b>3</b>
<b>1 Introduction</b>	<b>5</b>
1.1 Bulk-edge correspondence . . . . .	7
1.2 Topological photonics . . . . .	8
1.3 Microcavity polaritons . . . . .	9
1.4 Polariton lattices . . . . .	11
<b>2 Spin-orbit coupling in polariton molecules</b>	<b>15</b>
<b>3 Topological properties of one-dimensional polariton lattices</b>	<b>21</b>
<b>4 Topological properties of two-dimensional polariton lattices</b>	<b>27</b>
4.1 Edge states in polariton honeycomb lattices . . . . .	28
4.2 Engineering strain in polariton honeycomb lattices . . . . .	32
<b>5 Engineering of Floquet Hamiltonians in coupled fibre rings</b>	<b>37</b>
5.1 Floquet winding metals . . . . .	42
<b>6 Conclusions and perspectives</b>	<b>47</b>
<b>References</b>	<b>49</b>



# Foreword

This document presents a summary of the main research results in which I have been involved in the past few years in the field of topological photonics. This research is the outcome of a collective endeavour. It starts in 2012-2013 at *Laboratoire de Photonique et Nanostructures* (LPN) where I was a CNRS researcher working in close collaboration with Jacqueline Bloch. Joining her group in 2010 was a turning point in my career as it allowed me to get involved into the design and study of artificial photonic lattices. I arrived at the LPN at a sweet moment because Jacqueline Bloch in collaboration with Aristide Lemaître and Isabelle Sagnes had just developed a new technology capable of laterally etching semiconductor microcavities while preserving the optical properties. This breakthrough was the result of years of technological development on e-beam, etching and passivation optimisation. It opened fabulous possibilities in the design of one- and two-dimensional lattices, bringing polaritons to the realm of quantum emulation. Hand in the hand with Jacqueline, we jumped into the very exciting adventure of exploring the physics of polariton lattices with an unprecedented quality.

The development and study of polariton lattices was the main subject of the ERC Starting grant I was awarded in 2013. We first worked on the fabrication of polariton molecules of few sites and on one-dimensional lattices. We studied polariton condensation in flat bands, Fibonacci quasi-crystals and nonlinear polariton devices based on one-dimensional structures. In 2014 we fabricated a two-dimensional honeycomb lattice of coupled micropillars. This was a milestone for us because it was the first two-dimensional lattice ever fabricated via microcavity etching and it required some modifications of the technological processes employed so far. We went into the study of these lattices inspired by the remarkable transport properties of graphene.



### La parité dans les métiers du CNRS 2012

At about the same time, the first works on photonic lattices with topological properties were published by the groups of Mohammad Hafezi and Mordechai Segev. We were fascinated by how concepts issued from topology enabled new ways of manipulating light in lattices. From a fundamental point of view, topology was bringing a new perspective to the analysis of the properties of a system based on symmetries. I had the chance to participate in the summer program on "Synthetic Gauge Fields for Atoms and Photons" in Trento in 2013 and in the OSA incubator meeting "Topological Order with Photons" in Washington DC in 2014 in which the first generation of topological photonic effects were presented.

Inspired by the first results in the communities of atomic and photonic lattices we quickly focused on the study of topological properties of honeycomb lattices. Our work was pioneering in the observation of topological properties in orbital bands and in the engineering of unconventional Dirac cones for photons. The development of those concepts led us to the study of the topology of quasi-periodic lattices, to the implementation of artificial magnetism for polaritons and to the demonstration of the first laser in a topological edge state. The use of polaritons in the context of topological photonics opens very exciting perspectives thanks to the possibility of operating the system in the nonlinear regime, in which topological properties are expected to present quite exotic phenomena. This is a very active research direction today in our group and the main subject of the ERC Consolidator grant "EmergenTopo" that is running since June 2020.

In 2017, family reasons led me to move to the *Laboratoire de Physique des Lasers, Atomes et Molécules* (PhLAM) at the University of Lille, where I continue the very fruitful collaboration with Jacqueline Bloch and Sylvain Ravets, who joined her group also that year. The arrival at PhLAM was an extraordinary opportunity to learn new topics and initiate new collaborations. During my first four years at PhLAM I have established solid collaborations with colleagues with expertise in fields as diverse as nonlinear optics, ultrafast dynamics,

---

fibre systems and TeraHertz photonics. With Pierre Suret, we are implementing a new set-up for the ultrafast measurement of the polariton field in a single shot. This technique will allow us to measure the stochastic hydrodynamics of the polariton flow. With Stéphane Randoux, we have set-up a coupled fibre ring experiment that allows simulating Floquet-Bloch Hamiltonians acting on light pulses. We expect unveiling novel topological phases based on the periodic time modulation of the system. With Pascal Szriftgiser from PhLAM and Gaëtan Levecque, Yan Pennec, Marc Faucher and Guillaume Ducournau from IEMN we are working on the implementation of topological photonic crystals in the TeraHertz domain. All these research directions anticipate very exciting results in the upcoming years.

Addressing the wide variety of topics we have studied experimentally in the past few years, which go well beyond topological photonics, has been only possible thanks to very fruitful collaborations with a large number of theoreticians from many different countries. For all they taught to us, I would like to thank Eric Akkermans, Natalia Berloff, Iacopo Carusotto, Cristiano Ciuti, Alexandre Dauphin, Pierre Delplace, Alexey Kavokin, Anatoly Kamchatnov, Tim Liew, Guillaume Malpuech, Pietro Massignan, Gilles Montambaux, Tomoki Ozawa, Nicolas Pavloff, Simon Pigeon, Grazia Salerno, Sebastian Schmidt, Dimitry D. Solnyshkov, Gonzalo Usaj, Hakan Türeci, Michiel Wouters and Oded Zilberberg.

Among all these collaborators, I would like to mention two groups that have had a particularly strong influence in my work. Guillaume Malpuech and Dimitry D. Solnyshkov have been key actors in the understanding of polariton physics for the past two decades, particularly in the area of spin-orbit coupling in microcavities. They have produced some of the most original and imaginative ideas in the field, including the first prediction of a Chern insulator in a polariton lattice under a magnetic field. Their work has shown the tremendous potentialities of microcavity polaritons to explore remarkable lasing and nonlinear phenomena. I have had the great chance to collaborate with them since 2009. Going beyond polaritons, Iacopo Carusotto has been a tremendous inspiration in the field of fluids of light and topological photonics. Not only his discoveries and theoretical proposals have been enlightening and stimulating to bring this field further than we could have imagined, but also his methodology of work and his pedagogy when he discusses with experimentalists, have been illuminating. I have had the chance to collaborate with him since 2008 when we studied the superfluid behaviour of polaritons.

I would also like to highlight the many collaborations with other experimentalists: Ivan Favero, Rupert Huber, J.-M. Ménard, Maxime Richard and Thomas Volz. In particular, I had the chance to collaborate with Daniele Sanvitto at a time in which we were thrilled with the observation of a variety of polariton hydrodynamic features. We had a lot of fun doing those experiments both in Lecce and in Paris.

Finally, I need to thank all the PhD students, post-docs, engineers, and other collaborators that have taken part in the experimental work of the different groups in which I have worked since 2008: Claire Adrados and Romain Hivet at the LKB, Dimitri Tanese, Lydie Ferrier, Marco Abbarchi, Hai-Son Nguyen, Cris Sturm, Thibaut Jacqmin, Vera G. Sala, Peristera Andreakou, Marijana Milicevic, Félix Marsaut, Florent Baboux, Said. R. K. Rodriguez, Valentin Goblot, Philippe St-Jean, Nicola Carlon Zambon, Abdou Harouri and Luc Le Gratiet at the LPN/C2N, Omar Jamadi, Bastián Real, Albert Adiyatullin, Corentin Lechevalier, Cécilia Ouarkoub, Clément Évain, Clément Hainaut and Marc Le Parquier at PhLAM. They have shaped our research and strongly contributed to build the concepts that inspire us to go further.

### **Aim, structure and methodology of this document**

The aim of this document is to present a summary of the main results we have obtained in the area of topological photonics with polaritons and coupled fibre rings in the past few years. The first chapter introduces the subject and describes the main properties of polaritons in semiconductor microcavities and the methodology to fabricate polariton lattices. The subsequent chapters summarise briefly the main scientific results. The ordering of the chapters does not follow a historical timeline. We have preferred to organise each chapter according to the dimensionality of the explored system, which actually has strong implications on the kind of accessible topological properties. Each chapter introduces the specific sub-field and presents a summary of the main results obtained by our group. At the end of each chapter we cite the main scientific articles from our group related to its content. We first discuss the topological properties of single and few coupled micropillars in the presence of polariton spin-orbit coupling (Chapter 2). Next, we address the topological physics of one-dimensional polariton lattices (Chapter 3). Then we discuss our results in two-dimensional polariton lattices (Chapter 4). The final chapter before the conclusions is devoted to our recent achievements in a system of two coupled fibre rings, in which Floquet topological physics can be studied (Chapter 5). Finally, we discuss future perspectives.

*Alberto Amo García, July 2022*

# Chapter 1

## Introduction

Topology studies the properties of a system that remain unchanged under smooth local transformations. For instance, a loop in two dimensions can be described by the number of crossings it has, irrespective of their exact position and the local curvature of the loop. Similarly, the number of holes in a closed surface in three dimensions is conserved under smooth transformations. In these two simple examples, the number of crossings in the loop and the number of holes in the closed surface are integer numbers  $n$  that classify these objects into different topological classes ( $n = 1, 2, 3, \dots$ ). The topological invariant  $n$  does not change as long as a crossing or a hole are not created or destroyed in the loop and surface, respectively.

These ideas, originally developed in the context of mathematics, appeared to be very powerful to understand a new state of matter discovered experimentally in 1980: the quantum Hall effect [1]. The quantum Hall effect is characterised by the formation of equidistant flat bands, also known as Landau levels, in a two-dimensional electron gas under a strong magnetic field. When the Fermi energy is tuned at a Landau level, the material presents a significant longitudinal resistivity, and when it is tuned in-between the levels, it drops to almost zero. Simultaneously, the Hall (transverse) conductance becomes quantised in multiples of  $e^2/h$ , with  $e$  being the charge of the electron and  $h$  Planck's constant. This value of the conductance is independent of the length and shape of the semiconductor containing the two-dimensional electron gas and it is preserved even in the presence of disorder and impurities.

This surprising result was clarified in 1982 by D. J. Thouless, M. Kohmoto, M. P. Nightingale and M. den Nijs. In a seminal paper [2] they established the connection between the quantisation of the conductance in the quantum Hall regime in a square lattice and an integral involving the electronic eigenfunctions over the whole Brillouin zone in momentum space. The relevance of this result is that it showed that the quantised transport at the edges

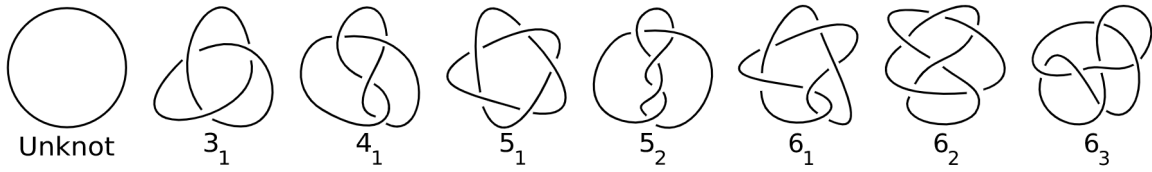


Figure 1.1: Table of prime knots with six crossings or fewer. From Wikipedia.

of the Hall bar is intimately related to the properties of the bulk of the system, and it is independent of the exact shape of the edges. The result of the bulk integral for each Landau band is an integer with properties very similar to those of a topological invariant. The invariant in this context was called the Chern number, and the formal relation between its value and the presence of edge states was demonstrated later by Y. Hatsugai and others [3, 4].

Those works triggered the curiosity of physicists working in the solid state community, who addressed other related questions. For instance, D. Haldane showed that a net external magnetic field is not needed to engineer topologically nontrivial bands and transport through edge channels [5]. Breaking time-reversal symmetry in the proper way is enough. A different effect was discovered by D. J. Thouless [6]. He showed that a quantised net current appears in a solid with an electronic filled band whenever the system is subject to a periodic varying potential. The magnitude of the transported charge is given Chern number of the filled band, and the phenomenon was coined a Thouless pump.

The topological properties of the above mentioned systems are intimately related to the breaking of time reversal symmetry, which sets the chirality of the one-way edge channels. Because electrons in these chiral channels cannot backscatter, their transport properties are very robust. In 2005 the family of topological materials was enlarged with a whole new class of electronic systems subject to spin-orbit coupling [7–9]. Conducting edge channels appear in the gap of the material with propagation in opposite directions for opposite spins. If time-reversal symmetry is preserved (absence of magnetic impurities) the coupling between the opposite spin channels is forbidden, and each spin class propagates without backscattering. The topological invariant in this situation is of  $\mathcal{Z}_2$  type and involves the two possible electronic spins [10]. New topological materials and phases continue to be discovered. Some examples include Floquet topological insulators in periodically driven systems [11–13], 3D Weyl semimetals [14], high-order topological insulators [15], topology of non-Hermitian systems [16], fragile topology [17], etc.

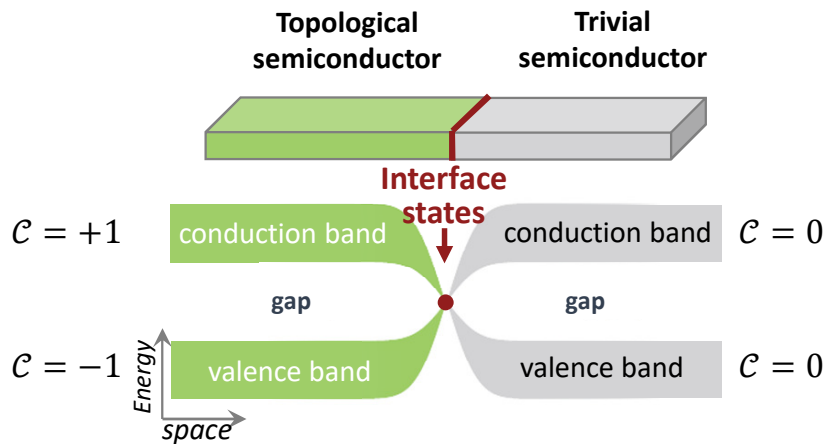


Figure 1.2: Formation of states in the gap at the interface of two materials whose bands possess different topological invariants.

## 1.1 Bulk-edge correspondence

As mentioned above, one of the most interesting properties of topological materials is the appearance of conducting channels at the edges of the material. The connection between a bulk topological invariant and the existence of those edge states has been formally studied in several theoretical works for different types of topological invariants (for a few examples see Refs. [3, 18, 4, 19, 13, 15]). The concept is schematically represented in Fig. 1.2. Let us have two two-dimensional materials with two bands separated by a gap, and let us assume that the gaps are centred at the same energy. The bands of each independent material are characterised by a topological invariant. If the invariants of the bands of the two materials are different, when pasting them together something special needs to happen at the interface. To regularise the topological invariants across the interface, the gap needs to close at the interface, such that when it opens again at the other side, the bulk bands have a different invariant. Therefore, at the energy of the bulk gaps there appear states spatially localised at the interface. Note that vacuum can be considered as a two band material with trivial bands separated by a very large gap, characterised by null topological invariant in the most typical definitions of invariants. Therefore, any single material with bands with topological invariants different from zero will show states localised at its edges.

This qualitative description of the bulk-edge correspondence permits understanding why the presence of edge transport channels is independent of the form of the interface: it depends only on the topology of the bulk materials at each side of the interface.

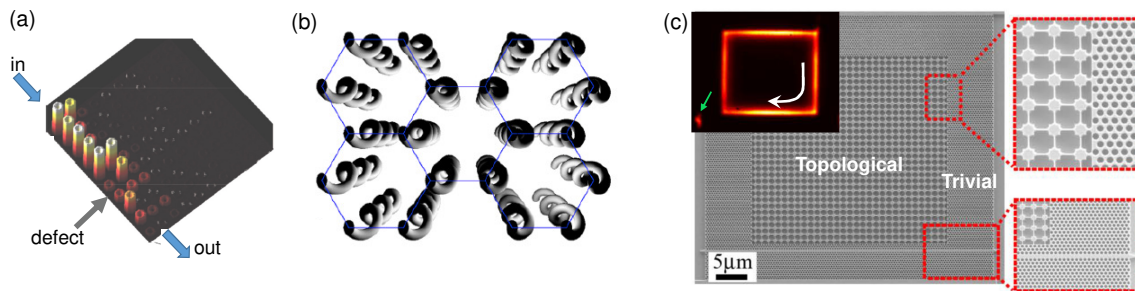


Figure 1.3: Examples of different photonic structures with topological properties. (a) Lattice of coupled ring resonators in Si implemented by the group of M. Hafezi [20]. The imaginary couplings around a plaquette emulate a gauge field resulting in directional edge transport around corners and defects. (b) Sketch of a honeycomb lattice of twisted coupled waveguides that implement the Haldane model for propagating photons, first realised by M. Rechtsman, A. Szameit, M. Segev and coworkers [21]. (c) Topological laser at  $1.5\mu\text{m}$  realised in a photonic crystal with a gyromagnetic material, by the group of B. Kanté [22]. The upper left inset displays the measured light emission, located at the edges between the trivial and topological lattices. Chirality of the emission is demonstrated by the fact that the output waveguide in the lower part of the photonic crystal shows emission mainly in the left region (green arrow).

## 1.2 Topological photonics

The possibility of exploring topological physics with photonic systems was first noticed in 2005 by F.D.M. Haldane and S. Raghu [23] in one of the seminal works of the field<sup>1</sup>. In that work the authors noticed that "The edge states are a property of a one-particle eigenstate problem similar to the Maxwell normal-mode problem, so they are replicated in the photonics problem." Haldane and Raghu discussed, in particular, the possibility of engineering a Chern insulator for photons in a lattice with broken time-reversal symmetry. Given that photonic lattices were already available, the only remaining issue to implement their idea was to break time reversal symmetry for photons. They suggested using magnetic materials whose index of refraction is different for opposite circular polarisations of light under an external magnetic field. This effect is extremely weak at visible or near infrared wavelengths, but it can be significant in the microwave regime. The first experimental implementation was reported in 2009 by the group of Marin Soljacic using a two-dimensional lattice of YIG resonators in the microwave regime under an external magnetic field, with the spectacular observation of propagation with negligible back scattering even around corners [24].

<sup>1</sup>A first version of the manuscript was posted on arXiv in 2005. The final paper was published in Phys. Rev. Lett. in 2008.

The field really took off in 2013 with the publications of Mohammad Hafezi and co-workers [20] and of Mikael Rechtsman and co-workers [21] in which they showed edge transport in two dimensional lattices of coupled waveguides at telecom and visible wavelengths, respectively. More importantly, those works did not rely on the breaking of time reversal symmetry to engineer the topological phases, which had been one of the main obstacles to develop the field in the photonics realm.

Since then, photonic systems have proved to be very versatile in the implementation of topological phases inspired from solid-state physics. Topological concepts can be very useful to design photonic devices that largely outperform traditional designs. Research in photonic systems has played a key role in understanding the symmetries behind the emergence of topological effects [25], in the discovery of anomalous Floquet phases [12, 26, 27], and in the first observations of Weyl points [14] and Fermi arcs [28] (see Refs. [29, 30] for detailed reviews). It has inspired genuine photonic phenomena such as topological lasing [31, 22, 32–36], the topology of PT symmetric non-Hermitian systems [37, 38], adiabatic pumping [39], the study of the effects of quantum optics in topological landscapes [40, 41], topological effect based on dissipative hoppings [42–44] and the direct measurement of the geometry and topology of energy bands [45–50]. More recently, lattices of photonic waveguides have allowed the observation of solitons and nonlinear effects in bands and gaps with non-trivial Floquet topology [51–55]. Topological concepts have provided a very efficient route to engineer transmission channels in photonic chips with very low losses [56, 20, 25], including in the THz regime [34, 57].

Probably, the greatest assets of photonic systems to address topological phenomena are (i) the possibility of engineering the photonic band structure in a very flexible way, in particular in two-dimensional lattices; (ii) the direct measurement of the eigenstates of photonic bands and the edge states in simple optical experiments; (iii) the use of active, dissipative and nonlinear optical materials to explore novel topological phenomenology. Some of their disadvantages are the relatively weak sensitivity of photons to external magnetic fields at optical frequencies, which complicates the study of elaborate topological phases with broken time-reversal symmetry, and the short photon lifetime of certain systems. The rather low value of photon nonlinearities in most microstructured materials is also a challenge to study topological superfluids and nonlinear topological phase transitions.

### 1.3 Microcavity polaritons

Our main contribution to the field has been to bring these concepts to the field of microcavity exciton-polaritons and to study the topological properties of various lattices. Microcavity

polaritons are particularly suitable to study topological phases in photonics. The engineering of lattices of coupled polariton micropillars enables the implementation of lattice Hamiltonians that are well-described by tight-binding models [58], which has been one of the most popular conceptual frameworks to study and to understand topological phases of matter. Simultaneously, the hybrid light-matter nature of polaritons makes them both sensitive to magnetic fields and subject to interactions.

Microcavity polaritons are light-matter quasiparticles that arise from the strong coupling between photons confined in a semiconductor planar microcavity and the excitonic excitations of a material embedded in the microcavity [59]. A typical structure consists of a cavity spacer of a few tens or hundreds of nanometers in thickness surrounded by an upper and a lower Bragg mirror. The latter are made of  $\lambda/4$  thick layers of two alternating dielectric materials with different refraction indices (see Fig. 1.4(a)), where  $\lambda$  is the operating wavelength of the cavity. The cavity spacer is usually designed for one of the lowest Fabry-Perot modes to be in resonance with the exciton line of a semiconductor material embedded in the central region of the spacer. Photons confined in the cavity excite an exciton (i.e. a bound electron-hole pair), which eventually emits a photon that stays trapped in the microcavity long enough to be re-absorbed, re-emitted, and so on. This regime is called "strong light-matter coupling" and is no longer described by excitons and photons independently, but by hybrid quasi-particles called cavity polaritons. The main signature of the light-matter coupling is the splitting of the previously degenerate exciton and photon resonances into two bands called upper and lower polariton branches.

Polaritons can be described as a combination of excitons and photons in the following way:  $|pol\rangle = \alpha |ph\rangle + \beta |exc\rangle$ , where  $\alpha$  and  $\beta$  are, respectively, the photon and exciton fractions. Their properties are directly related to those of their constituents, and their relative content can be tuned by designing the proper microcavity structure [59]. Thanks to their photonic part, polaritons eventually escape out of the cavity in the form of photons, which carry all the information on amplitude, phase, energy, polarization (spin) and coherence of the intracavity photon field. This makes spectroscopy of polaritons in photoluminescence experiments an ideal tool to characterise the polariton bands and modes. Actually, this is one of the main assets of polaritons compared to other photonic systems, which are typically restricted to a few observables. Moreover, the vertical confinement in the cavity splits the photon modes into transverse electric (TE) and transverse magnetic (TM) linearly polarized modes. The magnitude and polarisation orientation of the splitting depends on the momentum of polaritons in the plane of the cavity [60] and can, thus, be formalised as a spin-orbit coupling effect [61]. Chapter 2 will be devoted to this physics and its implication in the engineering of chiral effects in polaritons. In addition, as we will see below, it is

possible to fabricate one- and two-dimensional lattices by acting on the photonic part with different techniques [58].

From the excitonic component, polaritons inherit a "matter" part that has two major effects. First, since excitons are electronic excitations of the quantum wells, they possess a real spin, which is sensitive to external magnetic fields via a Zeeman shift. Polariton modes at visible wavelengths are therefore significantly more sensitive to magnetic fields than photons in regular materials. This is crucial to implement topological phases with broken time-reversal symmetry, like Chern insulators [62, 63, 33]. Second, Coulomb interactions between excitons result in significant repulsive contact interactions between polaritons. In the weak density limit, the interactions result in a  $\chi^{(3)}$  Kerr nonlinearity. Interestingly, interactions are polarisation dependent [64–67], and can be used to engineer nonlinear Zeeman shifts (see Refs. [68–70] and Chapter 2). Another crucial property is that polaritons demonstrate bosonic stimulated scattering and gain. These nonlinearities are so significant that have allowed the observation of optical parametric oscillation [71, 72], polariton Bose-Einstein condensation and lasing [73, 74], superfluidity [75], Bogoliubov-like excitations [76, 77], and dark [78–80] and bright solitons [81].

Different materials have been used to implement microcavity polaritons. Strong light-matter coupling has been reported in microcavities based on AlGaAs [82], CdTe [83], GaN [84], and ZnO [85, 86], in dielectric microcavities with embedded organic [87, 88] and two-dimensional materials [89, 90] (MoS<sub>2</sub>, MoSe<sub>2</sub>, 2D Perovskites etc.), and combinations of them [91–93], among others. Here we will exclusively use AlGaAs-based heterostructures grown by molecular beam epitaxy at the Center of Nanosciences and Nanotechnology in Palaiseau (France). The reason is that this kind of heterostructure presents the highest crystalline quality due to the almost perfect lattice match between the different alloys used to fabricate the microcavity, and results in polariton lifetimes of tens to hundreds of picoseconds. Quality factors above 300 000 have been reported by other groups [94].

## 1.4 Polariton lattices

As mentioned above, one of the main assets of microcavity polaritons to investigate topological phenomena is the possibility of engineering one- and two-dimensional lattices [58]. The polariton platform that has been the most flexible in this aspect is represented by microcavities based on AlGaAs semiconductors. By performing electron beam lithography and inductively coupled plasma etching of the epitaxially grown microcavity down to the substrate, it is possible to laterally confine photons and, therefore, polaritons, preserving a high enough quality factor at low temperatures (5-10 K). This technique was first introduced by the group

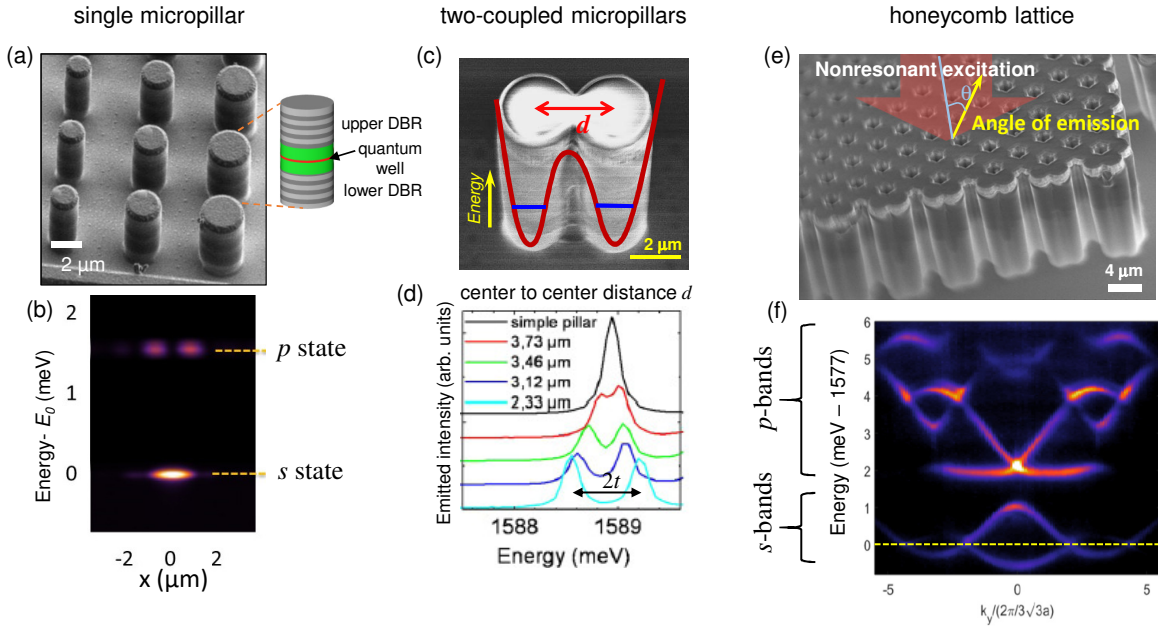


Figure 1.4: (a) Scanning electron microscope image of a series of individual AlGaAs-based polariton micropillars of different diameter. (b) Measured photoluminescence spectrum of the two lowest energy modes of a single micropillar. (c) Scanning electron microscope image of two (overlapping) coupled micropillars. (d) Measured spectrum of the lowest modes of two coupled micropillars of 4  $\mu\text{m}$  of diameter and different centre-to-centre distances, showing the emergence of bonding and anti-bonding modes whose energy separation increases with decreasing interpillar distance. From [97]. (e) Scanning electron microscope image of a polariton honeycomb lattice. (f) Measured spectrum in momentum space crossing the center of the Brillouin zone. The two sets of bands corresponds to the coupling of  $s$  and  $p$  modes, respectively.

of Manfred Bayer in microcavities in the weak coupling regime [95, 96]. The great leap forward in the technology used by the Center of Nanosciences and Nanotechnologies has been the development of passivation tools that prevent non-radiative recombination effects at the edges of the microstructures. To circumvent this difficulty, other groups have developed techniques such as metallic deposition on top of the upper Bragg mirror, partial etching of the upper mirror, partial mesa etching during the cavity growth, the use of open cavities with microstructured mirrors, acoustic lattices, nonlinear optical potentials and others. A detailed review of these techniques is available in Ref. [58].

A convenient building block to fabricate lattices is the semiconductor micropillar shown in Fig. 1.4(a). In this microstructure, photons are confined in the vertical direction by the Bragg mirrors and in the horizontal plane by total internal reflection due to the high index of refraction contrast between the semiconductor ( $n \sim 3.5$ ) and air or vacuum ( $n = 1$ ). As

polaritons are confined in the three dimensions of space, the spectrum of the micropillar shows a series of discrete  $s$ ,  $p$ ,  $d$ , ... gapped energy levels, represented in Fig. 1.4(b).

The lithographic mask can be designed to implement two overlapping micropillars, as shown in Fig. 1.4(c). The narrow section between the micropillars acts as a photonic barrier for the coupling of the polariton modes in the two different sites. For instance, if we assume that the lowest energy modes ( $s$ ) of the two individual micropillars have the same energy, the coupled system will display bonding and antibonding modes, separated in energy by  $2t$ , as sketched in Fig. 1.4(d). Here,  $t$  is the coupling strength, and it can be finely tuned by designing the appropriate center-to-center distance between micropillars [98, 97, 99].

The technique can be extended to fabricate one- and two-dimensional lattices with high flexibility. One of the advantages of using micropillars as a building block is that in the weak hopping limit, the polariton field dynamics  $\psi_n$  at each site in a lattice can be described with a Schrödinger-type equation using a tight-binding approach:

$$i\hbar \frac{\partial \psi_n}{\partial t} = \varepsilon_n \psi_n + \sum_{m \neq n} t_{n,m} \psi_m - i \frac{\hbar}{\tau} \psi_n + \text{source term.} \quad (1.1)$$

Here we consider a single mode of the micropillars (for instance the  $s$  mode) with onsite energy  $\varepsilon_n$ , which is controlled by the predesigned diameter of the pillars. The nearest-neighbour hopping  $t_{n,m}$  can be engineered by tuning the centre-to-centre distance between pillars [100]. The photon losses are captured by  $\tau$ , and the *source term* describes the excitation via an external laser source, which can take different forms depending on the resonant or non-resonant excitation configuration [59].

An example of a two-dimensional honeycomb lattice is shown in Fig. 1.4(e). The polariton bands can be measured in photoluminescence experiments, in which a non-resonant laser focused in the middle of the lattice excites electrons and holes in the quantum well. They relax down and form polaritons that populate the polariton bands. The real-space and angle-resolved detection of the emitted photons using a spectrometer and a CCD camera give access to the real- and momentum-space distributions of polaritons in the lattice. Figure 1.4(f) shows the lowest polariton bands of a lattice similar to that displayed in Fig. 1.4(e). The  $s$  bands exhibit Dirac crossings similar to those of electrons in graphene, while the upper  $p$  bands present a more elaborate structure [101].

A lower bound for the magnitude of the hoppings that needs to be engineered in a typical lattice is given by the polariton linewidth: to experimentally resolve the bands, the bandwidth –proportional to the hopping amplitude  $t$ – needs to be larger than the linewidth. This constraint actually places most polariton experiments out of the strict tight-binding limit of weak hopping. This can be readily seen in the asymmetry between the upper and lower

bands of both the  $s$  and  $p$  sets of bands shown in Fig. 1.4(f). Accounting for this asymmetry in a tight-binding model requires the addition of interband couplings, that is, the coupling of  $s$  and  $p$  modes (and of  $p$  and  $d$  modes, etc.) in adjacent micropillars, which can be effectively modelled as a next-nearest neighbour correction [100]. This deviation from a single mode per site has not prevented the study of a large number of topological effects in polariton lattices, well described by tight-binding Hamiltonians.

With this ingredients we can now address specific examples of topological phenomena we have studied in polariton lattices. Let us mention that a very complete review on the study of topological photonics with microcavity polaritons has been recently published [102]. That review, of which I am one of the leading authors, covers the work of most of the groups working in this field, and it has inspired part of this introductory chapter.

### **Relevant publications**

[30] T. Ozawa, H. M Price, A. Amo, N. Goldman, M. Hafezi, L. Lu, M. C Rechtsman, D. Schuster, J. Simon, O. Zilberberg, and I. Carusotto. *Topological photonics*, Rev. Mod. Phys. 91, 15006 (2019).

[102] D. D. Solnyshkov, G. Malpuech, P. St-Jean, S. Ravets, J. Bloch, and A. Amo. *Microcavity polaritons for topological photonics*, Opt. Mater. Express 11, 1119 (2021).

## Chapter 2

# Spin-orbit coupling in polariton molecules

The first studies in our group connected to topology involved the investigation of chiral modes in photonic molecules made of few coupled micropillars. These chiral modes arise from the coupling between the polarisation of light and the photon momentum in confined geometries. This coupling naturally appears in dielectric heterostructure due to the spatial inhomogeneities of the index of refraction [103]. In a planar microcavity, the index of refraction changes abruptly at the interface between the different materials that compose the heterostructure (Bragg mirrors, cavity spacer). As a result, the photon eigenmodes present transverse electric (TE) and transverse magnetic (TM) polarisations. The first corresponds to linear polarisation in the direction perpendicular to the propagation direction of photons within the plane of the microcavity, and the second to linear polarisation parallel to the propagation direction. In general, these TE and TM polarisation modes are split in energy everywhere in the two-dimensional momentum space except at  $k_{in-plane} = 0$  (normal incidence), where there is no distinction between the TE and TM geometries [60, 66, 61].

Figure 2.1(a) shows a scheme of the polariton dispersion of a planar microcavity made out of semiconductor Bragg mirrors. The TE and TM linearly polarised eigenmodes are clearly visible, with a splitting that increases from  $k = 0$  for low  $k$ . The splitting is strongly reduced for the lower polariton branch at large values of  $k$ , for which polaritons are mostly excitonic. The reason is that in GaAs-based materials, the exciton longitudinal-transverse splitting is usually much smaller than the photonic TE-TM splitting. The value of the splitting does not only depend on  $|k|$  but also on the design of the microcavity structure. Indeed, by modifying the thickness of the dielectric layers in the Bragg mirrors with respect to that of the cavity spacer, the TE-TM splitting can be made positive, negative or approximately zero [60].

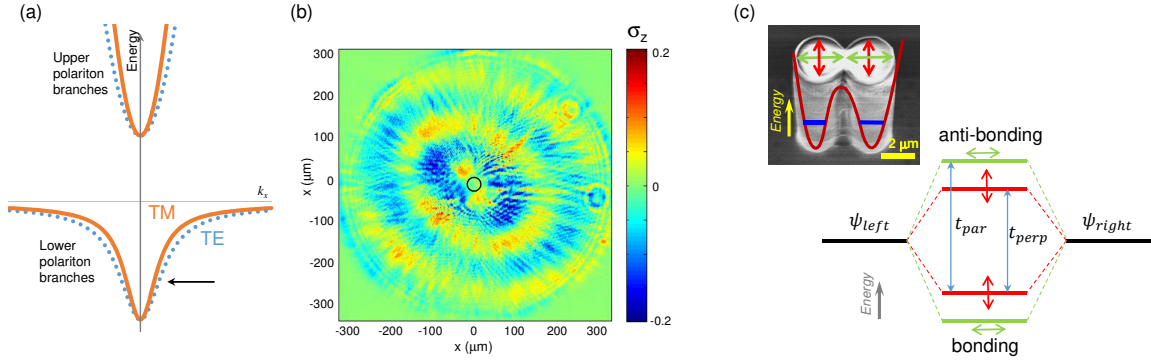


Figure 2.1: (a) Computed polariton dispersion of a planar microcavity as a function of  $k_x$  for  $k_y = 0$  including the TE-TM linear polarisation splitting. (b) Measured degree of circular polarisation  $\sigma_z$  of a polariton condensate expanding from an injection area marked by a circle at  $(x, y) = (0, 0)$ . The condensate is formed under non resonant excitation with a linearly polarised laser. Due to interactions with the reservoir, the condensate energy is 2 meV above the bottom of the lower polariton band. At the excitation point the condensate is linearly polarised. The polarisation precesses when propagating due to the presence of the TE-TM splitting, resulting in "waves" of circular polarisation. (c) Scheme of the effect of TE-TM splitting on a polariton molecule: the effective hopping is different for linear polarisations parallel (green arrows) and perpendicular (red arrows) to the link between the pillars.

Because the absolute direction of the TE-TM modes is determined by the propagation direction, the polarisation eigenmodes depend on  $\mathbf{k}$ . This can be seen as a form of spin-orbit coupling (SOC), a concept first introduced by the group of Alexey Kavokin and Guillaume Malpuech in 2004 [66, 61]. Its main consequence for the ballistic coherent propagation of polaritons is the precession of the polariton pseudospin (i.e., the polarisation) in a phenomenon known as optical spin Hall effect [61, 104, 105, 104, 106, 107]. An example produced in our laboratory in a GaAs planar microcavity is shown in Fig. 2.1(b). The nonresonant excitation injects a linearly polarised polariton condensate in a small region of about  $10 \mu\text{m}$ . Due to interactions between the condensate and the exciton reservoir, the condensate forms at an energy a few meV above the bottom of the lower polariton branch (arrow in Fig. 2.1(a)), accelerating the polariton gas in a radial expansion out of the excitation point. The TE-TM splitting results in the precession of the polarisation of polaritons as they propagate, giving rise to polarisation "waves". A similar polarisation precession was reported by other groups in Refs. [105, 104, 107, 68].

In 2013 we started studying the effect of the TE-TM splitting on polaritonic molecules made of coupled polariton micropillars. Particularly, in Ref. [108] we considered a closed hexagonal molecule (see Fig. 2.2(a)). One of the main advancements of this work was to introduce the description of the TE-TM splitting in a tight binding formalism. The main idea

is sketched in Fig. 2.1(c) for two coupled micropillars. The strength of the hopping of photons between adjacent pillars is different for modes polarised along ( $t_{par}$ ) and perpendicular ( $t_{perp}$ ) to the link between pillars. A phenomenological way of understanding the origin of this difference is to consider the different effective mass of TE and TM modes near the bottom of the polariton band in the planar cavity from which molecules are fabricated (see Fig.2.1)(a). This description we first introduced has been very successful in predicting the polarisation properties of polariton lattices [62, 109–113, 33, 114].

The spin-orbit coupling we have just discussed results in a very rich fine structure spectrum in a hexagonal molecule of coupled micropillars. The system is shown in Fig. 2.2(a). The lowest energy mode of each micropillar has cylindrical ( $s$ ) symmetry, similarly to the  $p_z$  electronic orbitals of the carbon atoms in a benzene molecule. If we disregard for the moment the polarisation degree of freedom, the coupling of the  $s$  modes results in four energy levels (see Fig. 2.2(b)). Due to the  $C_6$  symmetry of the structure, the eigenfunctions have a well defined angular momentum  $\ell = 0, \pm 1, \pm 2, 3$  and can be written in the form:  $|\ell\rangle = 1/\sqrt{6}\sum_m e^{i2\pi\ell m/6} |s_m\rangle$ , where  $|s_m\rangle$  is the  $s$  mode of each individual pillar. This means that the eigenmodes can be decomposed into spatial vortices in which the phase of the molecular mode when going around the molecule changes by  $2\pi\ell$ .

When the spin-orbit coupling is taken into account, the number of eignemodes is doubled. The  $\ell = 0$  and  $\ell = 3$  levels are now doubly degenerate in polarisation, but the  $\ell = \pm 1$  and  $\ell = \pm 2$  present a peculiar fine structure, schematically shown in Fig. 2.2(c)-(d). If we focus on the  $\ell = \pm 1$  manifold, we see that the lowermost ( $\psi_1$ ) and uppermost ( $\psi_4$ ) levels are linear combinations of states  $|-1, \sigma_+\rangle$  and  $|+1, \sigma_-\rangle$  orbital modes, in which the first index is the value of  $\ell$  and the second is the circular polarisation mode. The lowest state ( $\psi_1$ ) presents an azimuthal texture of linear polarisation when going around the molecule, while the uppermost ( $\psi_4$ ) has a radial linear polarisation texture. Therefore, these modes do not have any net vorticity. The two middle levels are the most interesting ones because each of them has an orbital vortex coupled to a circular polarisation component. Excitation of one of the modes would result in emission with a net chirality (i.e., net orbital angular momentum).

In a series of works [108, 115, 116] we have explored the lasing properties of the hexagonal molecule. When pumping the system with an out of resonance laser excitation that is linearly polarised, lasing gain favours the orbital mode with radial or azimuthal polarisation patterns [108]. In particular, in the manifold  $|\ell| = 1$  the azimuthal mode  $\psi_1$  has the longest lifetime and it is in which lasing is favoured (see Fig. 2.2(e)). At a different excitation power it is possible to trigger lasing in the  $|\ell| = 2$  manifold, in this case in the radially polarised mode.

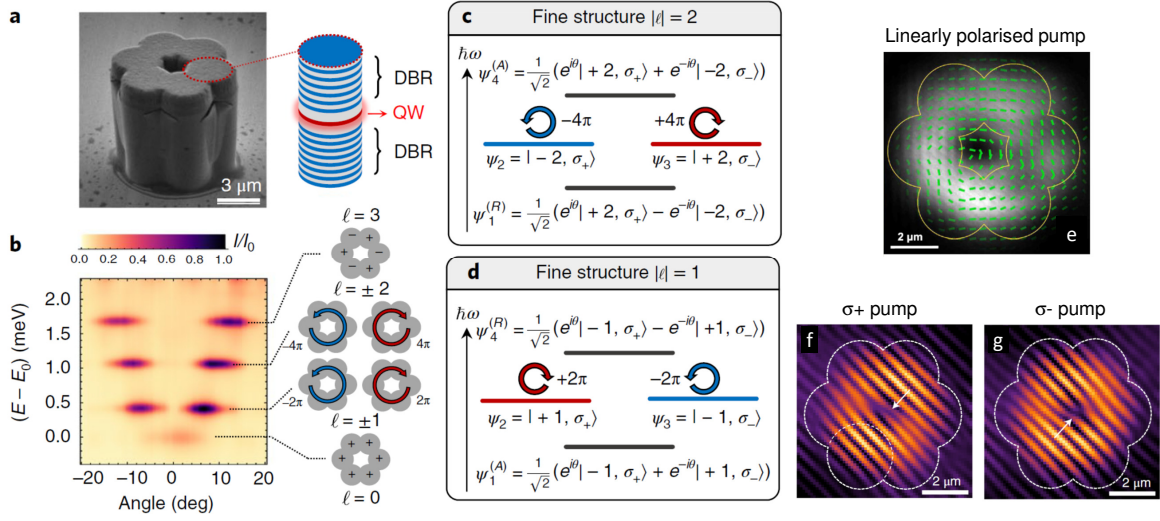


Figure 2.2: (a) Scanning electron microscope image of a hexagonal molecule of coupled polariton micropillars. (b) Energy and angle resolved photoluminescence of the lowest energy molecular modes and orbital scheme of the eigenmodes in the absence of spin-orbit coupling.  $E_0 = 1469.7$  meV. (c) Fine structure of the  $\ell = \pm 2$  manifold. (d) Fine structure of the  $\ell = \pm 1$  manifold.  $\theta = 2\pi/6$ . (e) Real space image of the emission from the lasing mode  $\psi_1$  of the  $\ell = \pm 1$  manifold under linear polarised pumping. Green segments show the measured direction of linear polarisation. (f)-(g) Emission of the lasing mode in modes  $\psi_2$  and  $\psi_3$  of the  $\ell = \pm 1$  manifold under circularly polarised  $\sigma_+$  and  $\sigma_-$  pumping, respectively. The observable fringes arise from the interference between the emission and a reference beam of the exact same frequency. They allow evidencing the orbital chirality of the modes via the presence of a phase dislocation at its center. (a)-(d) and (f)-(g) are extracted from Ref. [115] and measured in a microcavity with an InGaAs quantum well. (e) is extracted from Ref. [108] and measured in a microcavity with 12 GaAs quantum wells.

Interestingly, it is possible to trigger lasing in the chiral modes  $\psi_2$  and  $\psi_3$  of a given manifold, which we reported in [115]. To enhance the lasing gain of these modes, excitation with circular polarisation is required. This scheme creates a circularly polarised reservoir of excitons that induces an enhanced gain into the  $\psi_2, \psi_3$  modes of the  $\ell = \pm 1$  manifold with polarisation corresponding to that of the reservoir. Even though dephasing in the reservoir induces a fast depolarisation, it is possible to attain a degree of polarisation of the excitonic reservoir of the order of 10-20% at low temperatures. This is enough to favour lasing in one of those modes. Because the polarisation of the reservoir is determined by that of the nonresonant laser, it is possible to trigger laser into either the  $\psi_2 = |+1, \sigma_+\rangle$  mode or the  $\psi_3 = |-1, \sigma_-\rangle$ , which have opposite orbital chiralities, as shown in Fig. 2.2(f)-(g).

Note that the lasing in chiral modes reported in Ref. [115] and shown in Fig. 2.2(f)-(g) was achieved in a microcavity with a single quantum well in the weak coupling regime.

Lasing is triggered into one of the two degenerate chiral modes, but the system preserves time reversal symmetry in the sense that those modes remain degenerate. In microcavities in the strong coupling regime it is possible to break the time-reversal symmetry by taking advantage of the hybrid light-matter nature of polaritons and induce a splitting between those modes of opposite chirality. One possibility is to apply an external magnetic field parallel to the growth axis of the structure. The magnetic field induces a Zeeman splitting between excitons of opposite  $\pm 1$  spins, which couple to light with  $\sigma_{\pm}$  circular polarisation. Via the strong coupling, the Zeeman splitting is transferred to polaritons [117–120].

A different method is to take advantage of the polarisation dependence of polariton interactions to induce a nonlinear Zeeman splitting. The polarisation dependence of polariton-polariton interactions is a well documented phenomenon [65, 67, 121–124] whose origin can be found in the exchange terms of the exciton-exciton interactions [64]. Combined with the strong light matter coupling of polaritons, the excitonic exchange interaction results in a highly anisotropic polariton interaction: polaritons of same circular polarization interact much stronger than polaritons of opposite polarizations. Polarisation-dependent interactions also take place between polariton modes and the reservoir of excitons excited under nonresonant pumping [68, 69, 125, 70]. Therefore, by optically injecting spin-polarised carriers in the quantum wells it is possible to create an interaction-induced Zeeman splitting, i.e. different blueshifts for polaritons of the same and opposite polarizations than the exciton gas.

Recently, we employed this technique to induce a splitting between modes of opposite chirality [126]. Instead of using a hexagonal molecule, we studied a single micropillar. The  $p$  modes manifold in a single pillar has the exact same polarisation and orbital structure as the  $\ell = \pm 1$  manifold of the hexagonal molecule [127]. By injecting a circularly polarised reservoir we were able to demonstrate the energy splitting between modes  $\psi_2$  and  $\psi_3$ . In this case, time-reversal symmetry is broken and modes with opposite orbital chirality emit at different energies.

One of the most appealing applications of spin-orbit coupling and Zeeman effects in polariton lattices is the possibility of engineering Chern insulating phases. The idea was first proposed by Bardyn and co-workers [128, 63] and by Nalitov and co-workers [62], and realised experimentally by the group of Sebastian Klembt [33]. Still many intriguing topological phases with broken time-reversal symmetry are to be unveiled, in particular, in the nonlinear regime [129–132, 110, 111, 133]. Moreover, the possibility of locally varying the effective Zeeman field by using a combination of pump spots of different polarisations opens the possibility of engineering exotic gauge fields.

**Relevant publications**

[108] V. G. Sala, D. D. Solnyshkov, I. Carusotto, T. Jacqmin, A. Lemaître, H. Terças, A. Nalitov, M. Abbarchi, E. Galopin, I. Sagnes, J. Bloch, G. Malpuech, and A. Amo. *Spin-Orbit Coupling for Photons and Polaritons in Microstructures*, Phys. Rev. X, **5**, 011034 (2015).

[115] N. Carlon Zambon, P. St-Jean, M. Milićević, A. Lemaître, A. Harouri, L. Le Gratiet, O. Bleu, D.D. Solnyshkov, G. Malpuech, I. Sagnes, S. Ravets, A. Amo, and J. Bloch. *Optically controlling the emission chirality of microlasers*, Nat. Photonics, **13**, 283 (2019).

[116] N. Carlon Zambon, P. St-Jean, A. Lemaître, A. Harouri, L. Le Gratiet, I. Sagnes, S. Ravets, A. Amo, and J. Bloch, *Orbital angular momentum bistability in a microlaser*, Opt. Lett., **44**, 4531 (2019).

[126] B. Real, N. Carlon Zambon, P. St-Jean, I. Sagnes, A. Lemaître, L. Le Gratiet, A. Harouri, S. Ravets, J. Bloch, and A. Amo, *Chiral emission induced by optical Zeeman effect in polariton micropillars*, Phys. Rev. Research **3**, 043161 (2021).

## Chapter 3

# Topological properties of one-dimensional polariton lattices

One dimensional systems provide the simplest playground to study topological properties of lattices. They not only allow getting familiar with basic concepts in topology such as the bulk edge correspondence, but they also have specific properties that cannot be found in lattices of higher dimensions [10]. The most paradigmatic one-dimensional lattice with minimal topological properties is the Su-Schrieffer-Heeger (SSH) Hamiltonian. In the tight-binding limit, this lattice model is characterised by a unit cell with two sites with different intra- and inter-cell hoppings, respectively  $t$  and  $t'$  (Fig. 3(a)). For an infinite lattice, there are two possible choices for the unit cell (solid and dashed boxes in Fig. 3(a)). In both cases the eigenenergy spectrum is the same, distributed along two bands separated by a gap of magnitude  $2|t - t'|$ . However, the form of the eigenvectors and the topological properties are different in either case. The ambiguity is lifted in finite size lattices, in which the specific form of the termination sets the unit cell that describes the topological properties associated to that edge.

The Hamiltonian in momentum space can be written in the following form:

$$H = \begin{pmatrix} 0 & t + t'e^{-ika} \\ t + t'e^{+ika} & 0 \end{pmatrix} = d_x(k)\sigma_x + d_y(k)\sigma_y + d_z(k)\sigma_z. \quad (3.1)$$

This  $2 \times 2$  Hamiltonian is written in the basis of Wannier functions located in the A and B sites of the unit cell, with onsite energy equal to 0. As indicated in the right hand side of Eq. (3.1), the Hamiltonian can be written as the scalar product of a vector  $\mathbf{d}(k)$  and the vector of Pauli matrices  $\sigma_{x,y,z}$ .

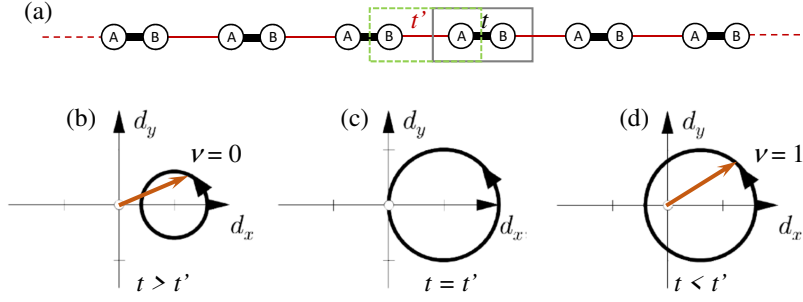


Figure 3.1: (a) Scheme of a lattice of coupled resonators with staggered hoppings  $t$  and  $t'$ . The two possible choices of unit cell are shown in solid and dashed squares. (b)-(d) Representation of the vector  $\mathbf{d}(k)$  in the  $x-y$  plane and the closed trajectory it follows when  $k$  is scanned between  $-\pi$  and  $\pi$  for different values of the staggered hoppings.

The eigenfunctions of Eq. (3.1) have the form  $\psi_{\pm}(k, m) = \sum_m \frac{1}{\sqrt{2}} (1, \mp e^{i\phi(k)})^{\dagger} e^{ikm}$ , where  $m$  is the unit cell number. The two components of the wavefunction describe the amplitude at the A and B sites, and  $\pm$  refers to the upper and lower bands, respectively. The phase  $\phi(k)$  follows from the equation:  $\cot \phi(k) = (t'/t) \sin^{-1} k + \cot k$ .

An invariant describing the topological properties of the above mentioned Hamiltonian can be written in multiple forms. The most straightforward is the winding number:

$$\nu = \frac{1}{2\pi} \oint_{BZ} dk \frac{d\phi(k)}{dk}. \quad (3.2)$$

$\nu$  can only take two possible values: 0 or 1. When  $t > t'$ , then  $\nu = 0$  and there are no states within the gap. However, when  $t < t'$ , then  $\nu = 1$  and a state appears at energy  $E = 0$  at each edge of the lattice. These states are of topological origin, they decay exponentially towards the bulk of the lattice, and their energy is robust against disorder and perturbations of the hopping amplitudes, as long as they are smaller than  $t, t'$ . The correspondence between the bulk invariant and the existence of edge states has been formally treated in several works [134, 19, 135, 136]. A graphical representation of the winding number is given by the evolution of the vector  $\mathbf{d}(k)$  in Eq. (3.1) when  $k$  goes from  $-\pi$  to  $\pi$ . As represented in Fig. 3,  $\nu$  is the number of times this vector winds around the origin in the  $[x, y]$  plane.

The simplicity of this model has been used to benchmark the possibility of implementing topological properties in a wide variety of systems. Probably, the first experimental implementation of this model and the observation of edge states come from the group of Zhigang Chen in a lattice inscribed in a photorefractive material [137]. The model has subsequently been explored in ultracold atoms [138, 139], microwave resonators [37, 50], photonic nanoparticles [140], coupled waveguides [38, 141] among other systems. In polariton systems, the SSH lattice was first proposed to explore the Kibble-Zurek mechanism

in polariton condensation [142]. Our group was the first to experimentally implement this model in 2017 [31], followed by experiments from other groups [143–145].

Polariton lattices offer the possibility of engineering the SSH model in a flexible way with direct access to the energy and eigenmodes of the system. Thanks to this feature, we have been able to directly measure the winding numbers described by Eq. 3.2. To do so, we employed a technique developed by Mondragon-Shem and coworkers [146] and by the group of Pietro Massignan [47, 147] based on the measurement of the *mean chiral displacement*:

$$C(t) = \sum_i \langle \psi_i(t) | 2\hat{\Gamma}_i \hat{Y}_i | \psi_i(t) \rangle, \quad (3.3)$$

where  $|\psi_i(t)\rangle$  corresponds to the instantaneous amplitude of the wave-function at the position of the *i*th site of the lattice,  $\hat{Y}_i$  is an operator that numbers the unit cell  $(0, \pm 1, \pm 2, \pm 3, \dots)$ , and  $\hat{\Gamma}_i$  is the sub lattice operator, which takes the value of +1 in the *A* sites and -1 in the *B* sites. In Refs. [146, 47, 147] it is shown that after an initial excitation of the SSH lattice at a single site, the quantity  $C(t)$  tends to the winding number  $\nu$  at long times. One of the interesting advantages of this technique compared to the measurement of the Berry phase when a wavepacket is accelerated in the bands [138, 46] is that it is based on a measurement of the spatial distributions, allowing to identify a winding number even in the presence of spatial disorder (as long as it preserves chiral symmetry) [139].

In the case of polaritons, if losses are smaller than the hopping amplitudes  $t, t'$ , Eq. (3.3) still applies and the mean chiral displacement can be directly extracted from the measurement of the emitted intensity in the steady state regime [49]. Figure 3.2(a) shows a polariton lattice with staggered distances between adjacent micropillars. This lattice implements the SSH hamiltonian when considering the *s* modes of each micropillar. Figure 3.2(b) shows the measured lowest energy bands, arising from the coupling of *s* modes, which display a gap. To measure the topological invariants using the mean chiral displacement technique, we excite the system at a single site with a non resonant laser that populates all the bands. The energy resolved emission in the steady state is shown in Fig. 3.2(c) and the energy-integrated intensity in Fig. 3.2(d). The time integrated mean chiral displacement  $\bar{C} = \lim_{T \rightarrow \infty} T^{-1} \int_0^T dx 2\Gamma(x)Y(x)I(x)$  for each definition of the unit cell can be computed directly from the multiplication of the measured intensity distribution and the chiral displacement operator  $\hat{\Gamma}_i \hat{Y}_i$ . Its value at each lattice site is represented by orange and blue lines in panel (e). The orange lines correspond to the definition of the unit cell with  $t > t'$ , while the blue lines to the case  $t < t'$ . For the first case  $\bar{C} = 0.05$  and for the second  $\bar{C} = 0.98$ , which very closely match the expected values of the winding numbers 0 and 1, respectively.

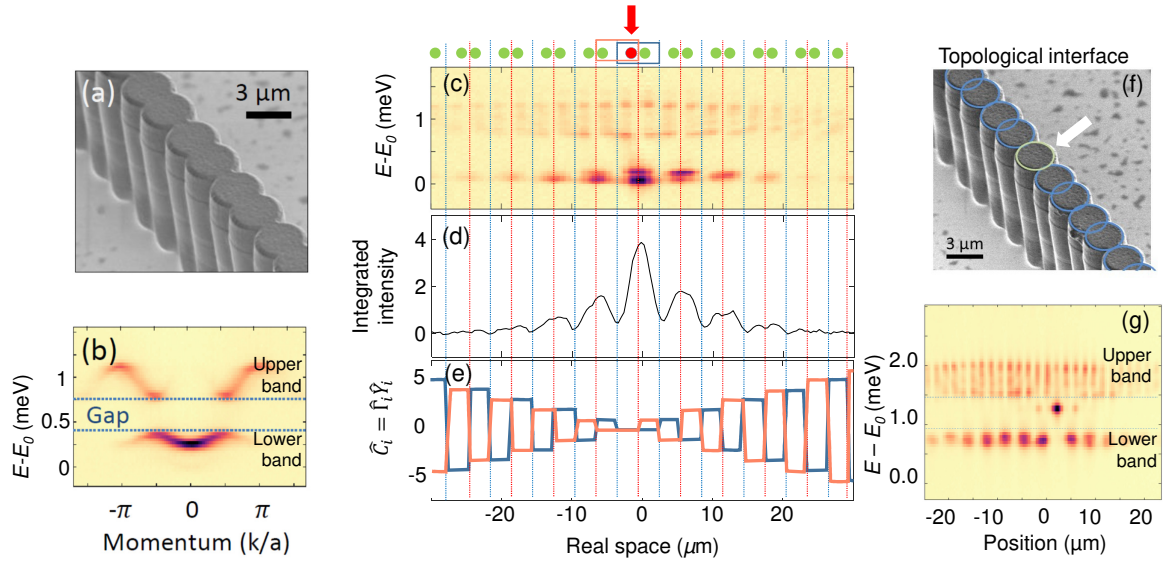


Figure 3.2: Mean chiral displacement and topological interface modes. (a) Scanning electron microscope image of an SSH lattice of coupled micropillars. (b) Measured  $s$  bands in a photoluminescence experiment showing the SSH gap. (c) Emitted intensity in real space as a function of the emitted energy. (d) Emitted intensity spectrally integrated over the  $s$  bands. (e) Value of the chiral displacement operator as a function of position in the lattice. Each coloured line depicts the chiral operator for the two possible definitions of unit cell shown as rectangular boxes in the scheme on top of panel (c). (f) Two SSH lattices of coupled micropillars with different topological phases connected by a weak link. The emitted intensity in (g) displays an interface state at an energy within the gap. Panels (c)-(e) have been adapted from Ref. [49].

The presence of edge states can now be evidenced in several ways. The most straightforward is to connect two SSH lattices with different winding numbers. This is the case illustrated in Fig. 3.2(f). The energy and spatially resolved emission shows the appearance of a state at the interface between the two lattices, whose energy is close to that of middle of the gap.

So far, we have discussed the properties of SSH polariton lattices from the perspective of the conservative Hamiltonian Eq. 3.1. The possibility of engineering gain and dissipation in this kind of lattices has been used to demonstrate very interesting properties such as interface mode enhancement [37] or additional robustness of the edge states at the PT symmetric point [148]. Our group evidenced the first laser in a topological edge mode using a polariton SSH lattice [31]. In order to enhance the topological gap, instead of using a lattice for the  $s$  modes like the one shown in Fig. 3.2, we used a zigzag lattice of equally spaced micropillars, which implements the SSH model for the  $p$  orbitals. Figures 3.3(b) and (c) show a scheme of the arrangement of orbitals in the sub-spaces of  $p_x$  and  $p_y$  orbitals, respectively. By looking at

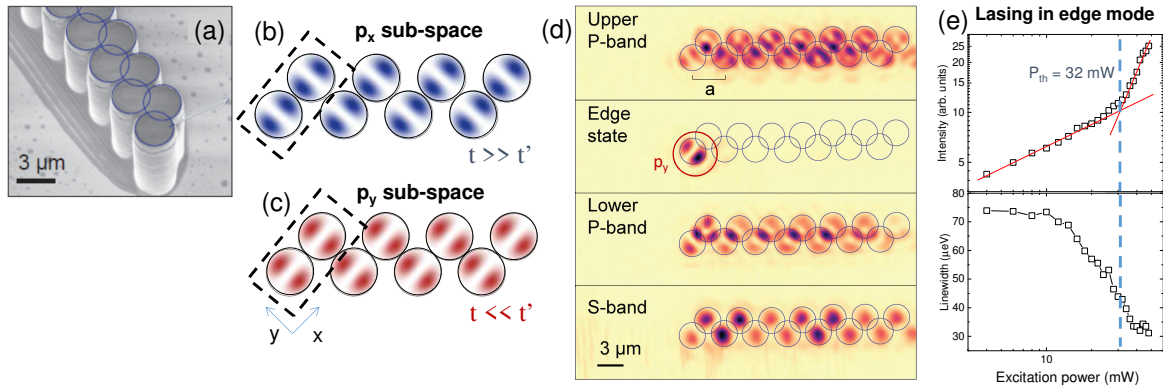


Figure 3.3:  $p$ -orbital SSH lattice. (a) A zigzag lattice of coupled micropillars. (b)-(c) Representation of the sub-spaces made of  $p_x$  and  $p_y$  orbitals. (d) Measured spatially resolved emission at the energies of the top of the  $s$  band, top of the lower SSH  $p$ -orbital band, topological edge mode in the middle of the gap, top of the upper SSH  $p$ -orbital band. (e) Integrated intensity and linewidth of the topological edge mode as a function of excitation power. The lasing threshold is at 32 mW. Adapted from Ref. [31].

the orbital overlap between adjacent micropillars, we can see that the  $p_x$  subspace alternates strong-weak hopping for the termination of Fig. 3.3(b). Therefore, this subspace corresponds to the phase  $\nu = 0$ . Simultaneously, sub-space of  $p_y$  modes (Fig. 3.3(c)) alternates weak-strong hoppings. It realises a topologically non-trivial SSH lattice with  $\nu = 1$ , and an edge mode is expected in the middle of the gap (see Fig. 3.3(d)).

When non resonant pumping the lattice close to the edge, the overlap of the pumped region with the edge mode is greater than with the bulk modes, resulting in lasing in the edge state. Almost simultaneously, the groups of Mercedeh Khajavikhan [149] and of Liang Feng [150] reported lasing in the topological edge modes of SSH lattices of coupled silicon microresonators. Lasing in the topological edge modes of two-dimensional lattices was also reported at about the same time [22, 32].

The flexibility in the design of the local polariton landscape has permitted the investigation of the topological properties of one-dimensional aperiodic potentials. In particular, in our group we have investigated a one-dimensional polariton lattice whose lateral confining potential follows a Fibonacci sequence [151]. Its spectrum presents a fractal structure with a series of gaps characterised by a topological invariant. We directly measured the presence of edge states associated to this invariant and its value in structures with an interface between two mirror images of a Fibonacci potential [152].

Let us end this chapter with a comment on the topological character of the SSH Hamiltonian. We have seen that the topological properties of this lattice model are related to the type of edge in a finite system. The topological invariants are, thus, well defined with respect to

specific terminations. This is a very important difference with other topological invariants in higher dimensions such as the Chern number or the  $Z_2$  invariant in two dimensions, which are unambiguously defined in the bulk and predict the number of edge states traversing the gap for any kind of edge. A very clarifying way of describing these features in the SSH model is to use the concept of "obstructed atomic limit", introduced in the context of solid state physics. It describes bands in which the Wannier centers are located in-between the lattice sites [153, 154], and cannot be continuously transformed into the bands of an atomic insulator. When cutting the lattice across these Wannier centres, edge states naturally appear. This description can be helpful to understand the appearance of edge state bands within the gap in two-dimensional trivial band systems, including 2D SSH lattices [19] and Dirac materials such as graphene, boron nitride (including valley Hall edge states), and the Wu and Hu model [155]. Further understanding of these features would be helpful to predict the appearance of midgap states in more elaborate lattices such as photonic crystals, which cannot be described with the tight-binding method due to the mixing of high orbital modes.

### Relevant publications

[31] P. St-Jean, V. Goblot, E. Galopin, A. Lemaître, T. Ozawa, L. Le Gratiet, I. Sagnes, J. Bloch, and A. Amo, *Lasing in topological edge states of a one-dimensional lattice*, Nat. Photonics **11**, 651 (2017).

[152] F. Baboux, E. Levy, A. Lemaître, C. Gómez, E. Galopin, L. Le Gratiet, I. Sagnes, A. Amo, J. Bloch, and E. Akkermans, *Measuring topological invariants from generalized edge states in polaritonic quasicrystals*, Phys. Rev. B **95**, 161114 (2017).

[49] P. St-Jean, A. Dauphin, P. Massignan, B. Real, O. Jamadi, M. Milicevic, A. Lemaître, A. Harouri, L. Le Gratiet, I. Sagnes, S. Ravets, J. Bloch, and A. Amo, *Measuring Topological Invariants in a Polaritonic Analog of Graphene*, Phys. Rev. Lett. **126**, 127403 (2021).

[156] N. Pernet, P. St-Jean, D. D. Solnyshkov, G. Malpuech, N. Carlon Zambon, Q. Fontaine, B. Real, O. Jamadi, A. Lemaître, M. Morassi, L. Le Gratiet, T. Baptiste, A. Harouri, I. Sagnes, A. Amo, S. Ravets, and J. Bloch, *Gap solitons in a one-dimensional driven-dissipative topological lattice*, Nat. Phys. (2022) DOI: 10.1038/s41567-022-01599.

## Chapter 4

# Topological properties of two-dimensional polariton lattices

Two-dimensional lattices are one of the most fascinating playgrounds for the study of topological effects in physics. In conservative systems without any external time modulation, two-dimensional systems can be classified into two main topological families: Chern insulators and spin-Hall topological insulators. The first family describes systems with gapped bands characterised by a topological invariant of the Chern type. The quantum Hall effect and the Haldane model are examples of this type of topological systems, and are characterised by the presence of unidirectional edge states in the gaps. These phases only exist when time-reversal symmetry is broken [10]. The second family was discovered in 2005 and corresponds to materials with a sizeable spin-orbit coupling. At the edges of the materials, two sets of edge states appear with opposite group velocities, each one for electrons of a given spin. The total Chern number of the bands is zero but the *spin Chern number* defined for a specific spin component may be different from zero. In this case, the topology is described by an invariant of the  $Z_2$  type [10]. In this family of topological insulators, the time reversal symmetry actually protects the topological order by preventing spin flips that would connect the spin edge states with opposite group velocity. Recently, the field of topological quantum chemistry introduced the use of crystalline symmetries to determine the topological character of a given set of bands, without the need to explicitly calculate Chern or  $Z_2$  invariants [153, 157].

Bringing these topological phases to photonics has been a significant challenge. First, photons are not very sensitive to external magnetic fields. Therefore, breaking time reversal symmetry is not an easy task at near infrared and visible wavelengths. The first observation of a photonic Chern insulator was reported in a lattice of magneto-optical rods in the microwave regime under an external magnetic field [24]. Later, Chern type edge states were reported

at near infrared wavelengths in the lasing regime, but with unresolvable gaps [22, 33]. For the family of topological phases arising from spin-orbit coupling, the bosonic nature of photons prevents the implementation of edge states fully insensitive to backscattering. Still, several geometries have been proposed and realised that mimic, to a certain extent, spin-orbit coupled topological insulators by engineering artificial gauge fields [20], by using crystalline symmetries [158, 40, 159] or the valley Hall effect [160].

Our first studies of the topological properties of two dimensional polariton structures were devoted to the honeycomb lattice. The coupling between the lowest energy modes of adjacent micropillars gives rise to two bands similar to the  $\pi$  and  $\pi^*$  bands of electrons in graphene [161]. The two bands touch at the Dirac points forming an ungapped spectrum, and the Chern number of the ensemble is, consequently, zero. Still, this system has a local Berry curvature that is different from zero close to the Dirac points. Additionally, it presents edge states of topological origin in the sense that they can be associated to an invariant of similar nature to that found in the SSH model, that is, associated to specific types of terminations of the lattice. We will discuss all these features below [18].

## 4.1 Edge states in polariton honeycomb lattices

In 2014 we realised the first honeycomb lattice of coupled micropillars with the aim of exploring all those properties in a fully controllable photonic simulator (see Fig. 4.1(a); Ref. [101]). A previous work from the group of Y. Yamamoto at Stanford had implemented a lattice based on a metallic layer with a hexagonal arrangement of holes grown on top of the upper mirror of the microcavity [162]. The metal modifies locally the index of refraction and produces a photonic potential. However, it was too shallow to evidence the presence of Dirac cones. The deep optical potential of our lattice of etched micropillars allowed unveiling not only the Dirac cones associated to the coupling of the lowest energy ( $s$ ) modes of each micropillar, but also the higher energy bands that arise from the coupling of  $p_x$  and  $p_y$  modes, see Fig. 4.1(b). Our work was the first to evidence them and one of the first in the optics community to realise *orbital* bands.

### **$s$ bands**

The  $s$  bands can be well described by the following tight-binding Hamiltonian in the basis of  $A$  and  $B$  sites of the honeycomb lattice (see Fig. 4.1(a)):

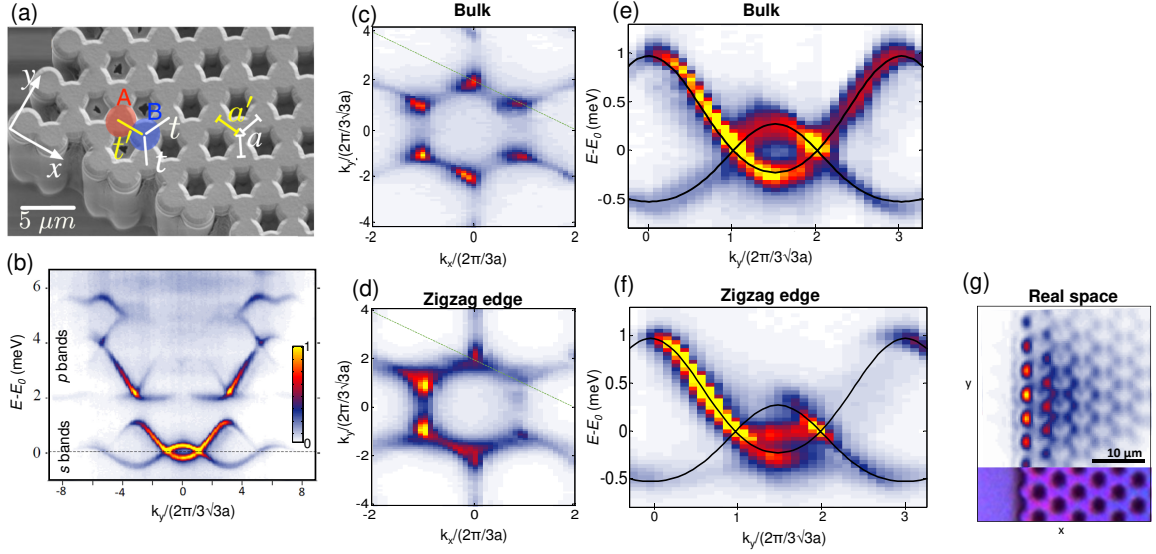


Figure 4.1: (a) Electron microscope image of a honeycomb lattice of coupled micropillars. (b) Measured photoluminescence in the bulk of the lattice as a function of  $k_y$  for  $k_x = 2\pi/(3a)$ . (c), (d) Momentum-resolved photoluminescence at the energy of the Dirac points when exciting the bulk (c) or the edge (d) of the lattice. (e), (f) Photoluminescence along the dotted green line in (c), (d), respectively, showing the dispersion of zigzag edge modes (d). (g) Real space emission at the energy of the zigzag edge states when exciting the lattice close to the edge. Figure adapted from Refs. [163] and [164].

$$H_s(\mathbf{k}) = \begin{pmatrix} 0 & f_s(\mathbf{k}) \\ f_s^*(\mathbf{k}) & 0 \end{pmatrix}, \quad (4.1)$$

where

$$f_s(\mathbf{k}) = t_s(1 + e^{i\mathbf{k}\mathbf{u}_1} + e^{i\mathbf{k}\mathbf{u}_2}) \quad (4.2)$$

with  $\mathbf{u}_1$  and  $\mathbf{u}_2$  being the lattice unit vectors,  $t_s$  the nearest-neighbour coupling, and we set the onsite energy to zero. The eigenvalues of Eq. 4.1 have two symmetric bands touching at the Dirac points. The asymmetry in energy visible in the measured bands in Fig. 4.1(b) comes from coupling of  $s$  and  $p$  modes in the lattice, and can be effectively described by adding next-nearest-neighbours hopping [101, 100].

Theoretical studies from the late 90s and early 2000s showed that edge states are expected to be present in graphene nanoribbons [165, 18, 166]. These edge states appear in the form of flat bands at *zero* energy connecting adjacent Dirac cones. Their origin can actually be traced to the topological properties of the bulk tight-binding Hamiltonian [18, 19]. To see that, let us take a closer look at Hamiltonian 4.1 and Eq. 4.2. Similar to the case of the SSH

lattice, the ambiguities in the selection of the unit cell in the case of a honeycomb lattice are settled in a ribbon by choosing a unit cell such that the edges of the ribbon are well reproduced by unit vector displacements. Along the edge of the ribbon, the lattice is periodic and a momentum  $k_{\parallel}$  parallel to the edge can be defined. The bulk Hamiltonian  $H_s$  can now be written as a function of  $k_{\parallel}$  and  $k_{\perp}$ . Different works [18, 134, 19] have shown that the number of zero energy edge states is given by the winding of the phase of the off-diagonal terms of the Hamiltonian  $f_s = |f_s| e^{i\phi(\mathbf{k})}$  along  $k_{\perp}$  perpendicular to the edge. Therefore, a winding number can be defined for each value of  $k_{\parallel}$ :

$$\nu(k_{\parallel}) = \frac{1}{2\pi} \int_{BZ} \frac{\partial \phi(k_{\parallel}, k_{\perp})}{\partial k_{\perp}} dk_{\perp}, \quad (4.3)$$

Let us first consider the case of an infinite ribbon in the  $y$  direction with zigzag edges. In this case,  $\mathbf{u}_1 = (3a/2, \sqrt{3}a/2)$  and  $\mathbf{u}_2 = (3a/2, -\sqrt{3}a/2)$ , and the off-diagonal terms of Hamiltonian 4.1 can be written:

$$f_s(k_x, k_y) = 2t_s \cos\left(\frac{\sqrt{3}}{2}ak_y\right) + t_s e^{i\frac{3}{2}ak_x}. \quad (4.4)$$

The winding number  $\nu(k_y)$  can be computed giving a value of 1 for  $|k_y| \in [2\pi\sqrt{3}a/3, 4\pi\sqrt{3}a/3]$ , and zero for the other values of  $k_y$ . This corresponds exactly with the regions in which zigzag edge states are experimentally observed (see Fig. 4.1(c)-(g)).

A more intuitive approach to the bulk-edge correspondence we have just described for zigzag edges can be formulated by noticing that for each value of  $k_x$ , the term  $f_s(k_x, k_y)$  Eq. 4.4 has the same functional form as the off diagonal elements of the SSH Hamiltonian 3.1. In Eq. 4.4, the role of the intracell hopping is played by  $2t_s \cos(\frac{\sqrt{3}}{2}ak_y)$  and that of the intercell hopping by  $t_s$ . Correspondingly, similarly to the SSH Hamiltonian, an edge state at zero energy appears for values of  $k_y$  such that  $2t_s \cos(\frac{\sqrt{3}}{2}ak_y) < t_s$ , which corresponds exactly to the condition stated above.

If the unit cell is now defined to accommodate bearded edges, the unit vectors  $\mathbf{u}_1$  and  $\mathbf{u}_2$  need to be modified accordingly and the winding number  $\nu(k_y)_{bearded}$  predicts the appearance of zero energy edgemodes in regions of  $k_y$  complementary to those for zigzag edges. Thanks to the direct spectroscopic access to the dispersions of polariton lattices we measured both the momentum space signatures of the zigzag and bearded edge states and their spatial distribution [167]. Figure 4.1(c)-(g) show the case of zigzag edges.

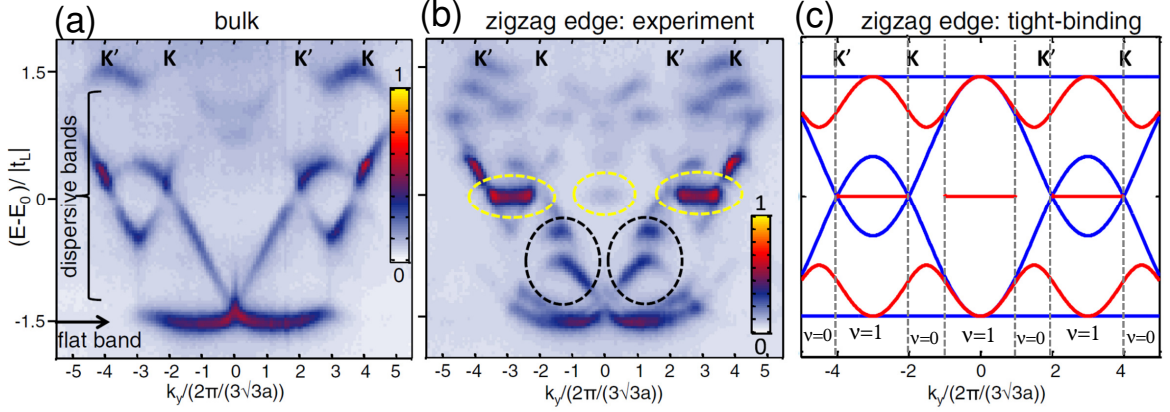


Figure 4.2: (a), (b) Measured photoluminescence dispersion of the  $p$  bands as a function of  $k_y$  for  $k_x = 4\pi/(3a)$  when exciting the bulk of the lattice (a) and the zigzag edge (b). (c) Calculated bands from the tight binding Hamiltonian of a ribbon. Blue lines are bulk modes while red lines are modes localised at the edges [163].

Our results went a step further than previous works in coupled waveguides [168] and lattices of microwaves resonators [169] by showing the eigenenergies of the edge states, inaccessible in those systems. In addition, we directly measured the winding numbers for the different values of  $k_{\parallel}$  using a coupled momentum-real space resolved technique giving access to the mean chiral displacement as a function of  $k_{\parallel}$ , see Ref. [49].

## $p$ bands

The orbital  $p$  bands present a richer edge state structure. Figure 4.2(a) shows the measured  $p$  bands when exciting the bulk of a lattice. The lowest band is almost flat, while the two middle ones are strongly dispersive with two band crossings similar to those at the  $K$  and  $K'$  Dirac points of the  $s$  bands. The highest energy band corresponds to a pseudo-flat band deformed due to the coupling to upper bands. These kind of bands were first discussed by Wu and Das Sarma in the context of ultracold atoms in an optical lattice [170], with the potential interest of engineering strongly correlated phases in the lowest energy flat band of the set. The bands can be qualitatively reproduced by a tight-binding Hamiltonian (see blue lines in Fig. 4.2(c)):

$$H_p = -t_L \begin{pmatrix} 0_{2 \times 2} & Q^\dagger \\ Q & 0_{2 \times 2} \end{pmatrix}, \text{ with } Q = \begin{pmatrix} f_1 & g \\ g & f_2 \end{pmatrix}, \quad (4.5)$$

where  $f_1 = \frac{3}{4}(e^{i\mathbf{k}\cdot\mathbf{u}_1} + e^{i\mathbf{k}\cdot\mathbf{u}_2})$ ,  $f_2 = 1 + \frac{1}{4}(e^{i\mathbf{k}\cdot\mathbf{u}_1} + e^{i\mathbf{k}\cdot\mathbf{u}_2})$ , and  $g = \frac{\sqrt{3}}{4}(e^{i\mathbf{k}\cdot\mathbf{u}_1} - e^{i\mathbf{k}\cdot\mathbf{u}_2})$ , and  $t_L < 0$  is the coupling of  $p$  modes oriented along the link between adjacent micropillars. The negative sign accounts for the antisymmetric phase distribution of the  $p_L$ -orbitals. We assume that  $p$  orbitals oriented perpendicular to the link do not overlap.

When exciting the structure close to a zigzag edge, new bands appear in the spectrum, marked by dashed lines in Fig. 4.2(b). They correspond to edge states, and can be classified into those at energy  $E_0$  (the energy of the  $p$  modes in an isolated pillar, assumed to be zero in Eq. 4.5) and dispersive modes at lower and upper energies (black dashed lines). Only those at zero energy can be directly linked to a bulk invariant. Indeed, by fixing a value of  $k_{\parallel}$ , the dependence of Hamiltonian 4.5 on  $k_{\perp}$  can be regarded as a one-dimensional model in the BDI (chiral orthogonal) class of the classification of topological insulators [10]. For this class, the treatment we performed above to predict the existence of edge states in the  $s$  bands can be generalised by calculating the winding of the phase  $\phi$  obtained from  $f_p \equiv \det Q = |\det Q| e^{i\phi(\mathbf{k})}$  [171]. By doing so, we find  $\nu(k_{\parallel}) = 1$  for  $k_{\parallel} \in [-2\pi/(3\sqrt{3}a), 2\pi/(3\sqrt{3}a)]$  for zigzag edges, and  $k_{\parallel} \notin [-2\pi/(3\sqrt{3}a), 2\pi/(3\sqrt{3}a)]$  for bearded edges. The regions in  $k_{\parallel}$  in which zigzag and bearded modes are present are complementary to those in the  $s$  bands [163]. There are not any zero energy edge state for armchair edges.

The dispersive edge states are a new feature of the  $p$  bands compared to the  $s$  bands. They are present both in zigzag, bearded and armchair edges [163]. However, we could not find a bulk invariant associated to their existence.

## 4.2 Engineering strain in polariton honeycomb lattices

The effects of mechanical strain on the electronic properties of graphene sheets have been a very important tool to engineer new kinds of Dirac cones. Only a few number of experiments have been able to show these effects in graphene and related materials [172, 173]. The reason is the extremely small lattice constant which makes it very difficult to control strain in a precise way. For this reason, synthetic metamaterials have been very successful in the study of these properties [174–176, 168, 177, 178]. One of the most interesting features of polariton lattices is, actually, the possibility of designing locally the hoppings of the lattice. Taking advantage of this property we engineered lattices with artificial strain with the goal of studying novel kinds of Dirac cones. We focused on unidirectional strain, that is, an anisotropy of the hoppings along only one direction. This can be done by keeping constant the vertical hoppings  $t$  in Fig. 4.1(a) and varying the horizontal hopping  $t'$ .

Let us start with homogeneous strain in which  $t'$  is made different from  $t$  but it takes the same value all over the lattice. In the  $s$  bands, when the "strained" hopping is increased,

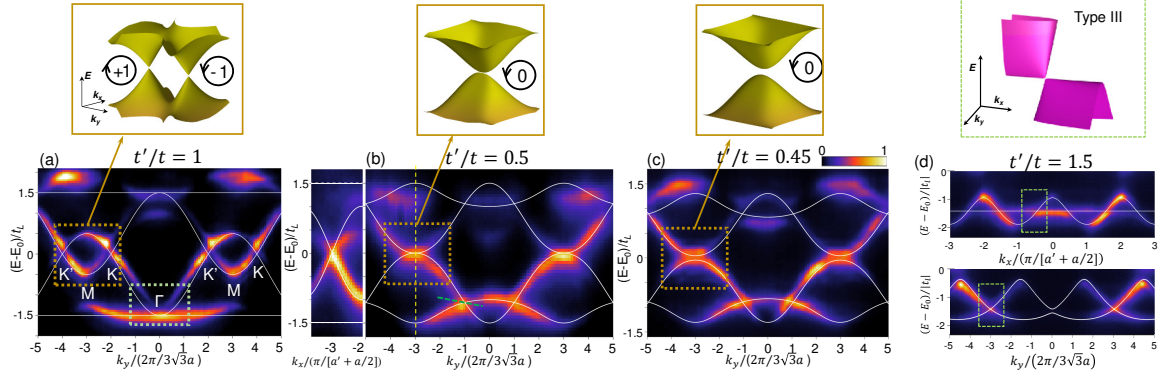


Figure 4.3: (a)-(c) Measured dispersion of the bulk  $p$  bands for different values of the engineered strain when  $t'$  is reduced. In all images,  $k_x = 2\pi/(a' + a/2)$ , where  $a$  and  $a'$  are the unstrained and strained interpillar distances shown in Fig. 4.1(a). The orange rectangle shows the merging of Dirac cones and gap opening (see calculated tight binding bands in the upper panels). In (b) and (c) the strain results in the emergence of tilted Dirac cones in the lowest two bands. (d) Measured dispersions for  $t' > t$  (upper panel:  $k_y = -2\pi/(\sqrt{3}a)$ , lower panel  $k_x = -0.5 \times 3\pi/(3a)$ ). Both dispersions cross at the type-III Dirac point highlighted in the dashed green box. The upper inset shows the tight-binding dispersion of the type-III Dirac cone. Adapted from Ref. [182].

the two Dirac cones at  $K$  and  $K'$  get closer to each other and end up merging at  $t' = 2t$  and opening a gap  $t' > 2t$ . At the merging point, the dispersion has a peculiar shape: it is massless (linear) along one momentum direction and massive (parabolic) along the opposite direction [179–181]. This kind of dispersion has received the name of *semi-Dirac cone* and it has strongly asymmetric transport properties, which we have experimentally evidenced [164].

In the  $p$  bands, the higher number of bands gives rise to a richer phenomenology when applying strain. When  $t'$  is now decreased with respect to  $t$ , the two Dirac cones at zero energy merge and give rise to a semi-Dirac cone at  $t' = (1/2)t$  (see Fig. 4.3(a)-(c)). At lower energies, at the contact point between the flat and dispersive bands, inclined Dirac cones appear, as evidenced in Fig. 4.3(b)-(c). Interestingly, when the "strained" hopping is increased, a new type of Dirac cone appears (see Fig. 4.3(d)). It combines a flat band and a linear dispersion with finite group velocity, which cross at the Dirac point. It has been speculated that the engineering of Dirac cones via strained graphene could be of interest to study analogue gravity physics. An interface between nanoribbons with normal and inclined Dirac cones would implement an event horizon for electronic excitations [183, 184]. By locally engineering the hoppings in the proper way, gravitational lensing analogue effects could also be engineered [185].

More sophisticated forms of strain can be used to realise synthetic magnetic fields in the spectral region close to the Dirac cones. The idea was first discussed in the context of carbon

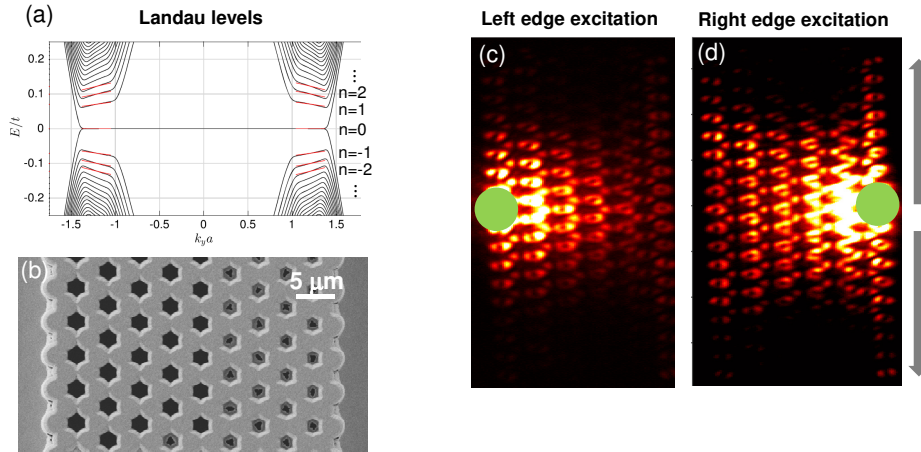


Figure 4.4: (a) Calculated energy bands of a ribbon presenting a linear gradient of hoppings along the  $x$  direction using the tight-binding method [189]. (b) Scanning electron microscope image of a polariton lattice implementing a linear gradient of hoppings in the  $x$  direction. (c), (d) Photoluminescence at the energy of the propagating edge states in between the  $n = 0$  and  $n = -1$  Landau levels of the  $p$  bands. When exciting the right edge, propagation along two helical edge modes is observed (d). Edge propagation is absent in the left edge (c). From Ref [190].

nanotubes [186] and then extended to planar sheets of graphene [187]. If a honeycomb lattice is strained radially into three directions separated by angles of  $120^\circ$ , an artificial magnetic field perpendicular to the sheet appears at each Dirac cone. The sign of the field is opposite at each  $K, K'$  valley. If the strain is engineered with the right spatial dependence, the spectrum is strongly modified giving rise to gapped Landau levels with the energy law characteristic of massless electrons:  $E_n \propto \pm \sqrt{|B|}$ , where  $B$  is determined by the strength of the strain. The presence of this field has been evidenced in graphene nanobubbles [172] and in a number of synthetic systems [175, 176, 188, 178].

Our goal in bringing this physics to polariton lattices was to engineer Landau levels in lattices that could be potentially used for the study of nonlinear optical effects and lasing in the presence of artificial magnetic fields and in flat bands. We followed the proposal of G. Salerno and co-workers who demonstrated that the artificial magnetic field could also be implemented in polariton lattices subject to uni-axial strain [189, 191]. Compared to the case discussed above of homogeneous strain leading to semi-Dirac cones, to engineer a constant valley dependent magnetic field we need to vary spatially the hopping  $t'$  in a linear way (i.e.,  $t' = \tau x$ ). The resulting bands are expected to display Landau levels (see Fig. 4.4(a)). We fabricated lattices with different hopping gradients along the  $x$  direction (an example is shown in Fig. 4.4(b)). Our experiments provided direct visualisation of the intensity distributions of the  $n = 0$  Landau level (not shown here, see also Ref. [178]) and the appearance of helical

edge states associated to the presence of the artificial magnetic field [190]. Interestingly, the presence of edge modes is associated to the specific terminations of the lattice [191]. For instance, in the zigzag-zigzag terminations of the lattice shown in Fig. 4.4(b), helical transport is only present along the right edge (Fig. 4.4(d)).

The high quality of the two-dimensional lattices fabricated at the Centre of Nanosciences and Nanostructures opens very exciting perspectives to go beyond the honeycomb lattice geometry and the linear physics we have presented in this chapter. For instance, taking advantage of the nonlinear properties of polaritons an interesting question is to study the modification of the topological properties due to particle interactions. This opens a whole new sub-field on the definition and role of topological invariants in presence of meanfield interactions, with first works starting to appear [53, 55, 192, 156].

### Relevant publications

[101] T. Jacqmin, I. Carusotto, I. Sagnes, M. Abbarchi, D. Solnyshkov, G. Malpuech, E. Galopin, A. Lemaître, J. Bloch, and A. Amo, *Direct Observation of Dirac Cones and a Flatband in a Honeycomb Lattice for Polaritons*, Phys. Rev. Lett. **112**, 116402 (2014).

[167] M. Milićević, T. Ozawa, P. Andreakou, I. Carusotto, T. Jacqmin, E. Galopin, A. Lemaître, L. Le Gratiet, I. Sagnes, J. Bloch, and A. Amo, *Edge states in polariton honeycomb lattices*, 2D Materials **2**, 034012 (2015).

[163] M. Milićević, T. Ozawa, G. Montambaux, I. Carusotto, E. Galopin, A. Lemaître, L. Le Gratiet, I. Sagnes, J. Bloch, and A. Amo, *Orbital Edge States in a Photonic Honeycomb Lattice*, Phys. Rev. Lett., **118**, 107403 (2017).

[193] M. Milićević, O. Bleu, D. Solnyshkov, I. Sagnes, A. Lemaître, L. Le Gratiet, A. Harouri, J. Bloch, G. Malpuech, and A. Amo, *Lasing in optically induced gap states in photonic graphene*, SciPost Phys. **5**, 64 (2018).

[182] M. Milićević, G. Montambaux, T. Ozawa, O. Jamadi, B. Real, I. Sagnes, A. Lemaître, L. Le Gratiet, A. Harouri, J. Bloch, and A. Amo. *Type-III and Tilted Dirac Cones Emerging from Flat Bands in Photonic Orbital Graphene*, Phys. Rev. X, **9**, 31010 (2019).

[100] F. Mangussi, M. Milićević, I. Sagnes, L. Le Gratiet, A. Harouri, A. Lemaître, J. Bloch, A. Amo, and G. Usaj. *Multiorbital tight binding model for cavity-polariton lattices*, J. Phys. Cond. Matt. **32**, 315402 (2020).

[190] O. Jamadi, E. Rozas, G. Salerno, M. Milićević, T. Ozawa, I. Sagnes, A. Lemaître, L. Le Gratiet, A. Harouri, I. Carusotto, J. Bloch, and A. Amo, *Direct observation of photonic Landau levels and helical edge states in strained honeycomb lattices*. *Light Sci. Appl.*, **9**, 144 (2020).

[164] B. Real, O. Jamadi, M. Milićević, N. Pernet, P. St-Jean, T. Ozawa, G. Montambaux, I. Sagnes, A. Lemaître, L. Le Gratiet, A. Harouri, S. Ravets, J. Bloch, and A. Amo. *Semi-Dirac Transport and Anisotropic Localization in Polariton Honeycomb Lattices*, *Phys. Rev. Lett.*, **125**, 186601 (2020).

[49] P. St-Jean, A. Dauphin, P. Massignan, B. Real, O. Jamadi, M. Milicevic, A. Lemaître, A. Harouri, L. Le Gratiet, I. Sagnes, S. Ravets, J. Bloch, and A. Amo, *Measuring Topological Invariants in a Polaritonic Analog of Graphene*, *Phys. Rev. Lett.* **126**, 127403 (2021).

## Chapter 5

# Engineering of Floquet Hamiltonians in coupled fibre rings

The implementation of lattice-based simulators in photonics has been a game changer for the study of new topological phenomena with no equivalence in solid-state materials. A very powerful example was the discovery in 2012 of anomalous Floquet topological phases in photonic step walks by Kitagawa and co-workers [12]. That work implemented a step walk version of the SSH lattice with staggered hoppings. In the first hopping event, photons split to adjacent sites of the lattice with a given splitting probability, while in a second step they were subject to a different splitting probability. Overall, the time evolution in this photonic lattice is periodic in time, with a period of two steps. The periodicity in time introduces a new symmetry with very important consequences in the energy spectrum of the system: the Brillouin zone is not only periodic in quasi-momentum, but also in the quasi-energy axis (Fig. 5.1). The spectrum of this model has two bands and two gaps, at  $E = 0$  and at  $E = \pm\pi$  (in normalised units). Topological edge states can appear at one of the gaps, both gaps or none of the gaps, as reported in several experimental and theoretical publications [194, 47, 195, 51], and illustrated in Fig. 5.1. Very interestingly, the full description of the presence of the edge states is not only given by the Zak phase in 1D and the Chern number in 2D, but also by a "Floquet" winding number that accounts for the topological properties imprinted by the periodic time modulation in the system, the so called "micromotion" within a time period [196].

This new topological property was first reported in one dimension in the experimental work of Kitagawa, and it quickly triggered the investigation of Floquet topological invariants in higher dimensions. In 2013, Rudner and coworkers published a proposal to implement a Floquet topological insulator in two dimensions, and provided an equation to calculate the associated winding number [13]. Additionally, if time reversal symmetry is broken in the

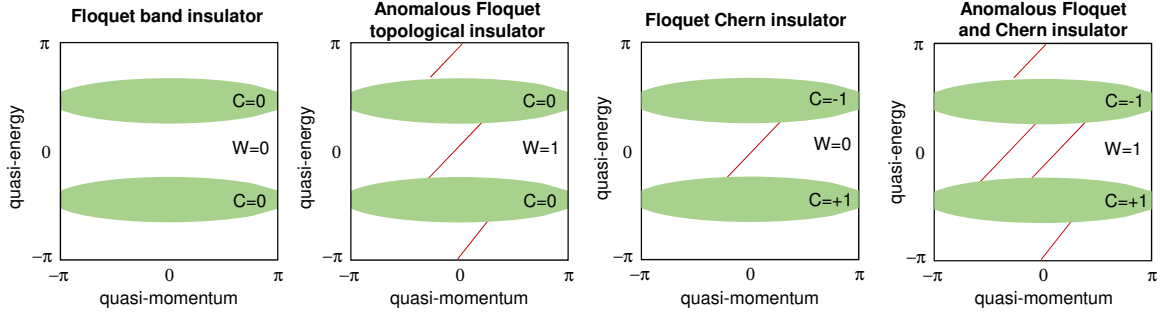


Figure 5.1: Examples of two-dimensional two band systems with Floquet-Bloch periodicity. Due to the periodic time modulation of the system the top and bottom parts of the quasi-energy spectrum fold into each other. Bands are represented in green, gaps in white and edge states in red.  $C$  indicates the Chern number of the bands and  $W$  the Floquet winding number of the middle gap.

proper manner, the total number of edge states in a gap is given by both the Floquet invariant and the Chern number (see Fig. 5.1-right panel).

The experimental realisation of this new topological phase in two dimensions, which was coined *anomalous Floquet topological insulator*, was first achieved in lattices of coupled waveguides [26, 27] and later in cold atomic gases [197]. Remarkably, the periodic modification in time of a physical system presents very rich phenomenology which goes beyond topological properties [195, 198, 199].

These features, hardly accessible in static polariton systems, motivated us to develop an experimental platform capable of addressing Floquet phenomena. Building on the know-how on fibre optics of the group of Stéphane Randoux and Pierre Suret at laboratory PhLAM, in 2018 we decided to implement an experiment based on a system of two-coupled fibre rings developed some years earlier by the group of Ulf Peschel in Jena [200–202, 51]. In this double ring system the time evolution of pulses of light can be controlled in a time-periodic manner using fast enough optoelectronic devices. At that time, the group of Peschel had hardly explored the topological aspects of the system [46, 203] and we found it perfectly fitted to investigate topological Floquet phases. Moreover, thanks to the possibility of accessing nonlinear effects in fibres [204], the system is suited to study nonlinearities in topological lattices.

We consider two fibre rings  $u$  and  $v$  of slightly different length as sketched in Fig. 5.2(a). The two rings are connected by a variable beamsplitter whose splitting ratio can be controlled electronically. A short pulse (2ns) of a 1.55 microns laser injected in one of the rings is split at the beamsplitter. After one turn, the pulses in each ring reach again the beamsplitter, but they do it at different times due to the difference in length of the rings. Each of them

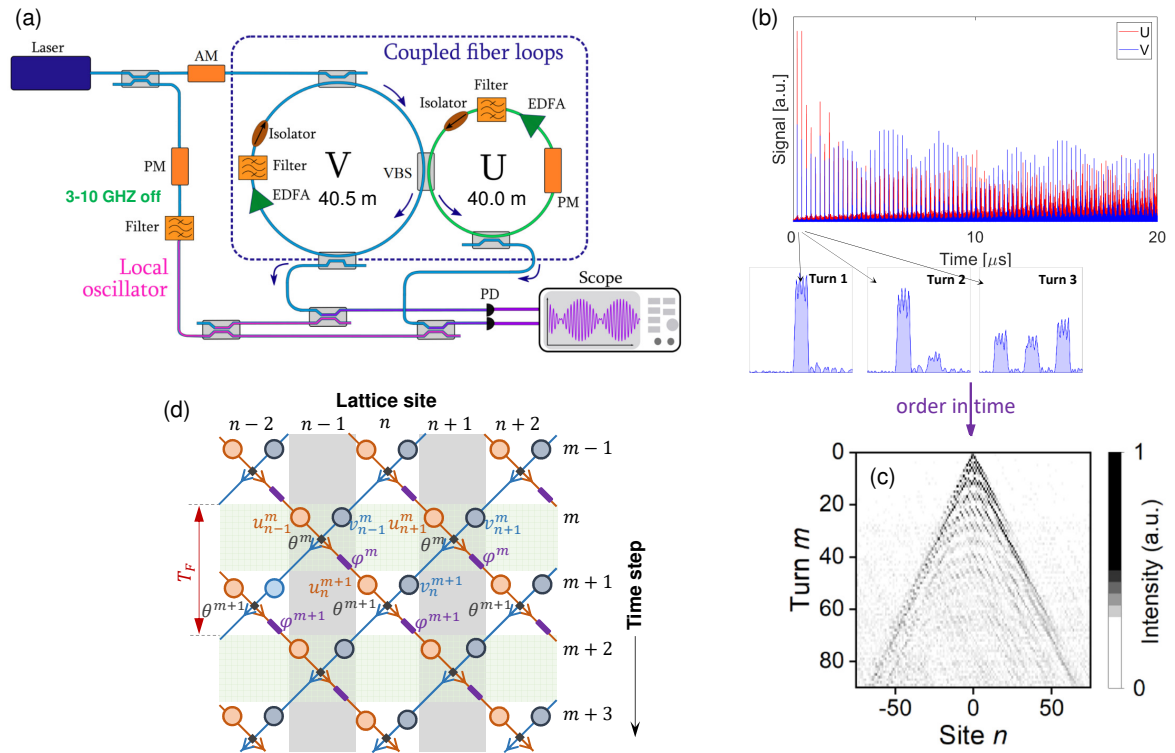


Figure 5.2: (a) Sketch of the two coupled rings setup. AM is amplitude modulator, PM is phase modulator, EDFA is Erbium doped fiber amplifier, VBS is variable beamsplitter and PD is photodiode. (b) Measured train of pulses in the  $u$  and  $v$  rings (red and blue, respectively) after excitation with a single pulse in the  $v$  ring. The inset shows the pulses in the  $v$  ring at time positions corresponding to the first three round trips. The oscillations on top of the pulses arise from the interference with the local oscillator. (c) Reconstructed spatiotemporal dynamics in the  $u$  ring when stacking the dynamics of each round trip in consecutive lines. (d) One-dimensional lattice subject to coherent split steps to which the dynamics in the double ring systems can be mapped.

splits, resulting in a train of two pulses in each ring. In the next turn, they split again and the delays between the pulses are such that the pulses coming from different rings start to interfere. Figure 5.2(b) shows the measured pulses on each ring as a function of time. The long time scale of several microseconds corresponds to tens of round trips. When zooming into a shorter time scale (lower insets of Fig. 5.2(b)) the different trains of pulses are apparent. In each train, the pulses are separated in time exactly by the time associated to the length difference between the rings.

The dynamics of the pulses in the two fibre ring system can be mapped into a one dimensional lattice subject to a coherent step walk in which a time step takes place at every round trip when the pulses split and interfere at the beamsplitter. The lattice is schematically

sketched in Fig. 5.2(d), and it has two sites per unit cell, corresponding to the amplitudes in the  $u$  and  $v$  rings. The "spatial position" of the pulses in the lattice is encoded in the temporal position within the train of pulses, while the step index is the round trip number. To compensate for the losses at the input and output beamsplitters, each ring has an Er-doped amplifier, allowing for the pulses to make hundreds of turns.

The pulse dynamics in the  $u$  and  $v$  rings can be written:

$$\begin{aligned} u_n^{m+1} &= (\cos \theta_m u_{n-1}^m + i \sin \theta_m v_{n-1}^m) e^{i\varphi_m} \\ v_n^{m+1} &= i \sin \theta_m u_{n+1}^m + \cos \theta_m v_{n+1}^m, \end{aligned} \quad (5.1)$$

where  $m$  is the round trip number and  $n$  is the "spatial" position of the pulses in the lattice.  $\cos \theta_m / \sin \theta_m$  are the variable beamsplitter splitting ratios. Additionally, in one of the rings we add a phase shifter that adds a phase  $\varphi_m$  to the pulses. Interestingly, this phase provides an additional periodic parametric dimension ( $0 < \varphi_m < 2\pi$ ). We continuously measure the light in each ring using a fast photodiode connected to a high bandwidth oscilloscope.

To get the eigenvalues and eigenmodes of the system we can apply the Floquet-Bloch ansatz to Eqs. 5.1:

$$\begin{pmatrix} u_n^m \\ v_n^m \end{pmatrix} = \begin{pmatrix} U \\ V \end{pmatrix} e^{-iEm/2} e^{ikn/2} \quad (5.2)$$

where  $U$  and  $V$  are the normalised complex amplitudes of the eigenmodes in the  $u$  and  $v$  rings,  $E$  is the quasi-energy and  $k$  the quasi-momentum. In the simplest case of a fixed 50/50 beamsplitter ( $\theta_m = \pi/4$ ) and  $\varphi_m = 0$ , the lattice system has two bands and the eigenvalues read:

$$\cos(E) = \frac{1}{2}(\cos(k) - 1) \quad (5.3)$$

The amplitude of the eigenvectors has the form:

$$\frac{V}{U} = \frac{i}{\sqrt{2}e^{ik/2}e^{iE/2} - 1}. \quad (5.4)$$

The trains of pulses shown in Fig. 5.2(b) have been measured in the 50/50 beamsplitter configuration and  $\varphi_m = 0$ . After ordering the trains by round trip time  $m$ , we obtain the spatiotemporal diagram of Fig. 5.2(c). In our system the rings have an average length of 40 m and a length difference of 0.55 m. This means that the round trip time is 205 ns and the spatial period of the lattice corresponds to 2.7 ns. The injected pulses are 1.7 ns long. Our rings are

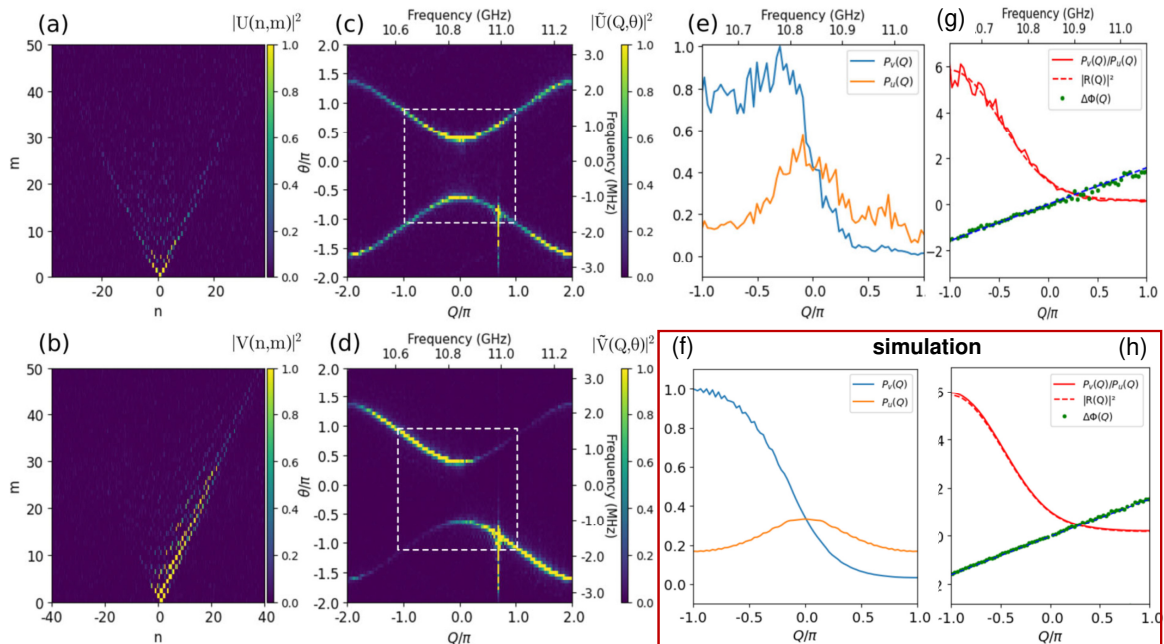


Figure 5.3: (a)-(b) Spatio-temporal dynamics measured in the  $u$  and  $v$  rings for 50/50 beamsplitter and  $\varphi_m = 0$  for excitation in the  $v$  ring with a single pulse. (c)-(d) Band structure computed from the Fourier transform of (a) and (b). The dashed rectangle displays the first Brillouin zone. (e) Measured amplitude square of the eigenvectors in each ring as a function of the quasi-momentum for the upper band. (f) Same as in (e) extracted from the simulations of Eq. 5.1. (g) Red line: measured ratio of the amplitude square  $v(k)/u(k)$  in the upper band. Green line: measured relative phase  $\phi(u(k)) - \phi(v(k))$  in the upper band. (h) Ratio of amplitudes and phase difference in the upper band computed from simulations of Eq. 5.1. Adapted from Ref. [205].

much shorter than those used by the groups of Peschel and Szameit [42], with lengths on the order of few kilometres and pulse lengths on the order of hundreds of nanoseconds. Our choice requires much faster electronics to chop the pulses and to measure the dynamics, but it also allows directly measuring the band structure of the lattice. One of the developments we have done is to combine the output of the fibres with a local oscillator detuned in frequency by several GHz from the wavelength of the laser used to generate the pulses. In this way, an interference signal on top of the pulses is observed (see inset of Fig. 5.2(b)), which contains information on the relative phase between pulses within a given time step  $m$ , and in-between time-steps. The band structure can be directly measured by doing the Fourier transform of the spatiotemporal diagram in which the measured pulses have interfered with the local oscillator [206], as shown in Fig. 5.3(c)-(d).

The dispersions obtained from the Fourier transform of the spatiotemporal dynamics have information not only on the eigenvalues as a function of the quasi-momentum, they also

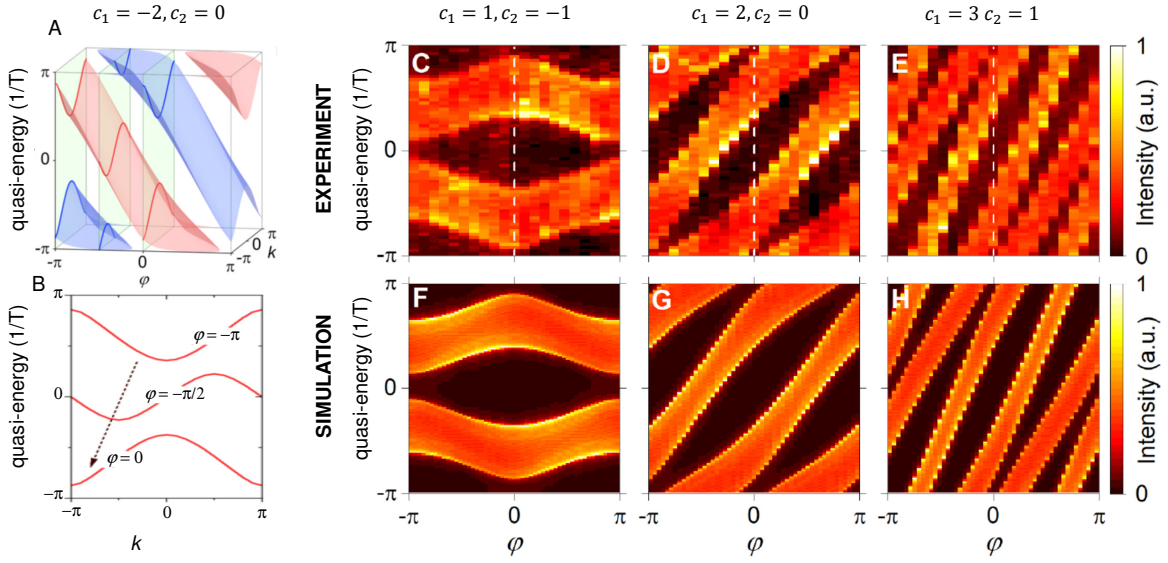


Figure 5.4: (a) Analytically computed two-dimensional band dispersion of a Floquet winding metal. (b) Band dispersions of the red band in (a) for selected values of  $\varphi$ . (c)-(e) Measured band dispersions as a function of  $\varphi$  for different windings related to the different values of  $c_1$  and  $c_2$ . (f)-(h) Band dispersions obtained from the simulation of the time evolution equations. Adapted from Ref. [205].

contain information on the amplitude and phase of the eigenvectors. Figure 5.3(e) shows the measure amplitude square of the excited modes in both rings. By analysing the complex angle of the measured dispersions for the  $u$  and  $v$  rings it is possible to extract the phase difference between  $u$  and  $v$  of each eigenvector of each of the two bands. The result of this operation is displayed in Fig. 5.3(g) green dots. In this case, we observe a linear increase of the phase difference from  $-\pi/2$  to  $\pi/2$ , which is well reproduced both by applying the same procedure to spatiotemporal simulations with identical initial conditions to those of the experiment (green dots in Fig. 5.3(h)). The measured phase difference also matches very well the analytical value extracted from Eq. 5.4. These results were reported in Ref. [206].

An interesting feature of the Floquet-Bloch lattice we are considering is that the amplitude of the eigenmodes is not the same for the  $u$  and  $v$  sites of the unit cell (see Fig. 5.3(c)-(f)). This is in strong contrast with the usual static lattices in the tight binding limit, in which the Bloch eigenmodes have the same weight in both sub-lattice sites.

## 5.1 Floquet winding metals

In the situation described above we have considered a lattice model subject to a step walk with the same lattice parameters at all time steps ( $\theta_m = \pi/4$ ;  $\varphi_m = 0$ ). Still the discrete

nature of the evolution allows a description based on the Floquet-Bloch theorem:  $H(t, x) = H(t + \tilde{m}T, x + \tilde{n}a)$ , where  $\tilde{m}, \tilde{n}$  are integers,  $T$  is the time period of the quantum walk, usually labelled Floquet period, and  $a$  the spatial period. In the coupled fibre ring lattice, using the definition of time step of Fig. 5.2(d), i.e., each round trip, the Floquet period is two steps. This can be easily seen in Fig. 5.2(d), where two time steps are needed to recover the same lattice positions.

We can now modulate in time the step walk parameters in order to investigate more elaborate lattice models. A very interesting one appears when we employ different splitting ratios at each of the two time steps within a Floquet period, and when we add alternating values of the phase shift  $\varphi_m$  in one of the rings. Specifically, the coupling between rings alternates between  $\theta_1$  and  $\theta_2$  and  $\varphi_m$  between  $\varphi_1 = c_1\varphi$  and  $\varphi_2 = c_2\varphi$ , where  $\varphi \in [-\pi, \pi]$ , and  $c_{1,2}$  are integer coefficients.

For a fixed value of  $\varphi$  the system is one-dimensional. But if we consider the  $\varphi$  as a parametric periodic dimension, the system becomes two-dimensional with eigenenergies [207]:

$$E_{\pm}(k, \varphi) = \pm \arccos \left[ \cos \theta_1 \cos \theta_2 \cos \left( k + \frac{c_1 + c_2}{2} \varphi \right) - \sin \theta_1 \sin \theta_2 \cos \left( \frac{c_1 - c_2}{2} \varphi \right) \right] + \frac{c_1 + c_2}{2} \varphi, \quad (5.5)$$

where  $\pm$  applies to the upper and lower bands.

In collaboration with the group of Pierre Delplace we showed that this model presents an exotic band structure [207]. When  $\theta_1 \neq \theta_2$  the two bands are gapped in the sense that they do not touch, but they can traverse the entire quasi-energy Brillouin zone if  $c_1 + c_2 \neq 0$ . This situation is illustrated in Fig. 5.4(a) for  $\theta_1 = \pi/4 - 0.4$ ,  $\theta_2 = \pi/4$  and  $c_1 = -2$ ,  $c_2 = 0$ . Since the bulk states exist at all energies, its spectrum can be identified with that of a metal [208]. Figure 5.4(c)-(e) shows three different experimental band realisations with different band windings governed by different values of  $c_1$  and  $c_2$ . In these experiments, reported in Ref. [205], the band dispersion in momentum space for each value of  $\varphi$  was recorded and represented in a  $\varphi$ -quasi-energy diagram. The winding metal bands are revealed, and well reproduced by simulations (Fig. 5.4(f)-(h)).

The lattice model we have just introduced has the particularity of having two different topological properties. The first one is the usual anomalous phases of Floquet lattices introduced by Rudner and coworkers in Ref. [13]. To evidence it, we prepare an interface between two regions with different Floquet topology (see Fig. 5.5(a) for the topological phase diagram). When injecting an initial pulse at the interface, presence of a localised state is revealed (Fig. 5.5(b), (c)). The measured band structure as a function of  $\varphi$  is displayed in Fig. 5.5(d) and it clearly shows the appearance of bands of edge states. The different

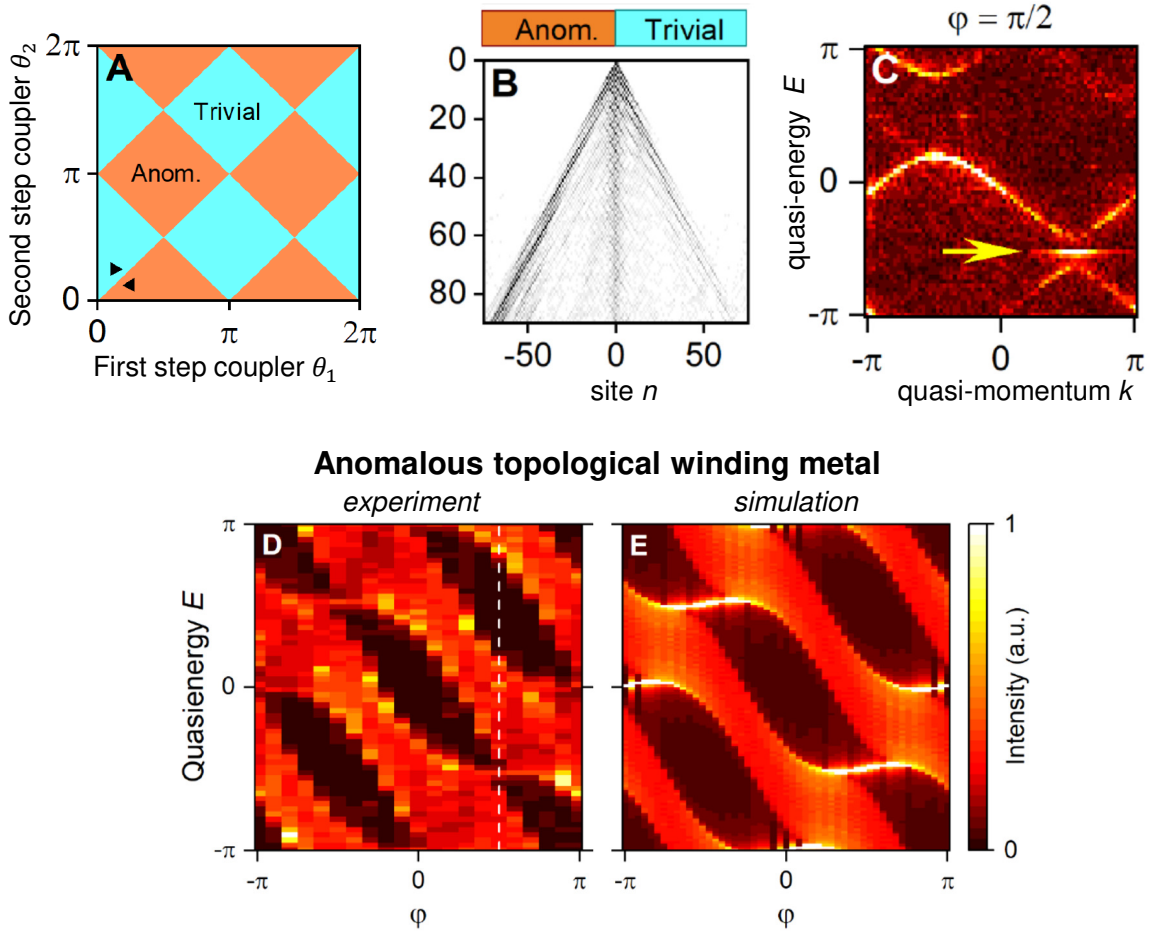


Figure 5.5: (a) Phase diagram of Floquet topological phases as a function of the splitting parameter in the first ( $\theta_1$ ) and second ( $\theta_2$ ) steps. (b) Measured spatiotemporal dynamics when injecting a single pulse at the interface between two one-dimensional lattices with different splitting parameters at the two steps, for  $c_1 = 1$ ,  $c_2 = -3$  and  $\varphi = \pi/2$ . The splitting parameters are marked with triangles in (a). Localisation of light at the interface unveils the presence of a localised state. (c) Fourier transform of the heterodyned emission shown in (b). The presence of an interface can be identified in one of the gaps (yellow arrow). (d) Measured full band diagram as a function of  $\varphi$ . (e) Band diagram from simulations of Eqs. 5.1. Adapted from Ref. [205].

topological phases are governed by the values of the  $\theta_1$  and  $\theta_2$  (the splitting ratios), and are separated by regions in which one of the gap closes. The presence of the anomalous Floquet edge states is independent of the winding of the bands, set by the values of  $c_1$  and  $c_2$ .

The second topological property is original to the winding metals and it is based on the band holonomy that makes the bands wind through the Brilluoin zone, which is simultaneously periodic in quasi-momentum, quasi-energy and  $\varphi$  [209]. The winding of the bands is illustrated in the example shown in Fig. 5.4(b) for one of the bands: when  $\varphi$  increases, the

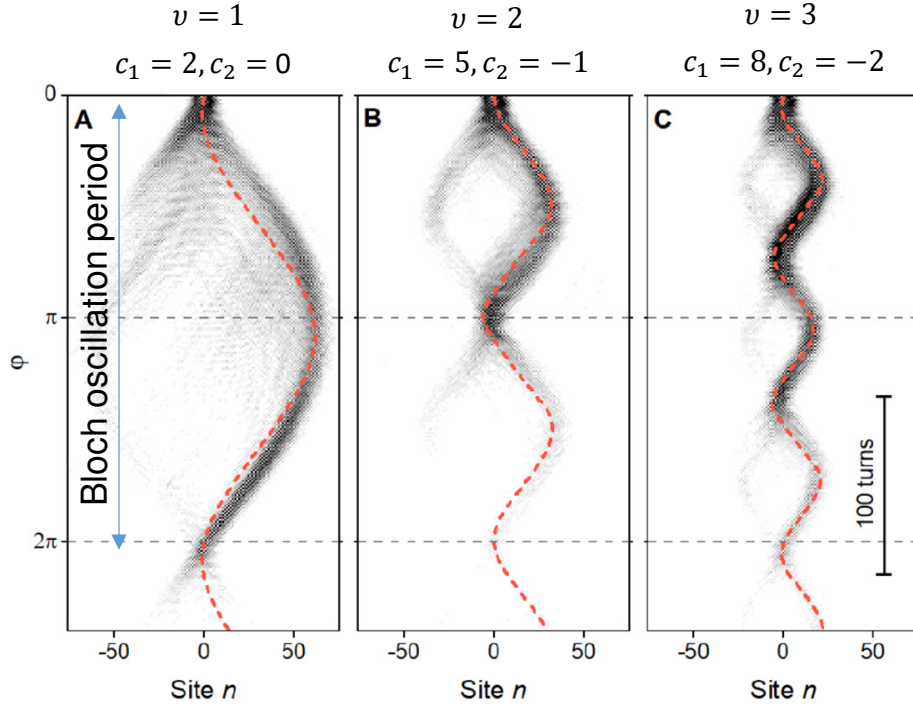


Figure 5.6: (a)-(c) Measured Bloch oscillations when injecting a wavepacket at  $k = 0$  in the upper band and  $\varphi$  being linearly increased (left axis). The three panels correspond to three different band windings, mentioned on top of each panel. From Ref. [205].

band is shifted both in energy and quasi-momentum. The winding can be characterised by a topological invariant defined as [11]:

$$v = \sum_{j=\pm} \frac{1}{2\pi} \int_0^{2\pi} d\varphi \frac{\partial E_j}{\partial \varphi} = \frac{1}{2\pi i} \int_0^{2\pi} d\varphi \text{Tr} \left[ U_F^{-1} \frac{\partial U_F}{\partial \varphi} \right] = c_1 + c_2. \quad (5.6)$$

In the second equality we have written Eq. (5.6) in terms of the Floquet operators  $U_F$  just to point out that the winding number can be related to them. A detailed description of the system in terms of Floquet operators can be found in Ref. [207].

One of the most spectacular phenomena we have found in this system is that the winding of the bands manifests in the shape and period of Bloch oscillations when a wavepacket is accelerated along the  $\varphi$  dimension. Figure 5.6 shows three examples of a wavepacket initially prepared at  $k = 0$  in one of the bands as  $\varphi$  is increased. The wavepacket dynamics is periodic with the periodicity of the Brillouin zone in  $\varphi$  dimension ( $2\pi$ ). In addition, it presents suboscillations whose number within a period ( $\varphi : 0 \rightarrow 2\pi$ ) is directly the winding number  $v$ . The amplitude of the suboscillations is not constant, as can be seen from a careful

analysis of Fig. 5.6(c). Note that the number of suboscillations, which directly reflects the winding number, is robust to the presence of disorder in the couplings [207].

We have shown the experimental implementation of a band model with several topological properties which manifest in very different wavepacket dynamics. One interesting question is if new topological properties can emerge from the combination of different topological properties, how to couple them, and what real or synthetic space dynamics can be expected. For us, the fact that we managed to realise experimentally such complex systems has been very motivating to address other topological physics including nonlinear effects, topological pumps, non-Hermitian configurations and the measurement of topological invariants.

### Relevant publications

[207] L. K. Upreti, C. Evain, S. Randoux, P. Suret, A. Amo, and P. Delplace, *Topological Swing of Bloch Oscillations in Quantum Walks*, Phys. Rev. Lett., **125**, 186804 (2020).

[206] C. Lechevalier, C. Evain, P. Suret, F. Copie, A. Amo, and S. Randoux, *Single-shot measurement of the photonic band structure in a fiber-based Floquet-Bloch lattice*, Commun. Phys. **4** 243 (2021).

[205] A. F. Adiyatullin, L. K. Upreti, C. Lechevalier, C. Evain, F. Copie, P. Suret, S. Randoux, P. Delplace, and A. Amo, *Multitopological Floquet metals in a photonic lattice*, arXiv :2203.01056.

# Chapter 6

## Conclusions and perspectives

The field of topological photonics has bloomed in the last decade. This success is rooted on three complementary aspects. First, the assets of photonic systems to emulate solid-state Hamiltonians has allowed the study of lattices with engineered topological properties with a very high degree of control. Photonic systems have played an important role in the discovery of novel topological phases, such as the Floquet topological insulators, in the measurement of topological invariants, and in the use of crystal symmetries to design topology-inspired photonic crystals with high transmission channels. Second, the field of topological photonics has witnessed the development of novel concepts with a genuine photonic aspect. Examples include the implementation of topological lasers and the discovery of non-Hermitian topological phases. Third, the concept of topology inspired photonic crystal has allowed the design of photonic circuits with a very small footprint and extraordinary transmission properties. These topological circuits may play an important role in the design of integrated active devices in a large range of wavelengths, from the visible to the THz.

One of the most stimulating current challenges in the field of topological photonics is the understanding of the influence of nonlinear effects on the emergence of topological phases [210]. One of the hallmarks of band topology is the non-locality of topological invariants, which are most often defined over the entire Brillouin zone. Nonlinear effects are usually local properties, arising from close interactions between particles. As a consequence they tend to break the spatial symmetries of the system, which are at the core of the most extended descriptions of topological phases. First experimental efforts have been directed to the study of nonlinear localised solutions in lattices with underlying topological properties [54, 53, 55, 192], including in our group [156]. Recently, an intriguing experiment by the group of Alexander Szameit has shown the self formation of an edge channel at high localised

photon densities in a lattice that is topologically trivial in the linear regime [53]. A different, very interesting configuration is that of "emergent topology": an extended, interacting photon fluid in a trivial lattice breaks time-reversal symmetry for its density excitations, which present a topological gap with chiral edge states [156]. Polaritons can play an important role in the experimental exploration of these intricate topological phases.

Polariton lattices are an excellent platform to study new physics arising from the interplay of drive, dissipation and nonlinearity. In this direction, several works of our group have already explored the physics of first order phase transitions in a bistable micropillar [211], localisation and antilocalisation in a driven dimer [212–214] and in a polariton lattice [215], and dissipative solitons in 1D wires [216] and in an SSH lattice [156]. Resonant laser drives on selected sites of a lattice allow forcing the local phase of the system opening the possibility of engineering frustrated modes. In the context of lattices with topological properties, these features might give rise to novel dynamics around points of large Berry curvature in a band.

Lastly, our work on couple fibre rings opens the door to studying even more exotic situations. Adding time periodicity to a spatial lattice enlarges the parameter space for the engineering of topological phases. For instance, it would be very interesting to study the interplay of anomalous Floquet phases and Chern phases, which can be directly implemented in the fibre ring. Going beyond periodically driven systems, the physics of lattices with quasiperiodic driving in time remains largely unexplored. Understanding the topological properties induced by such exotic drivings is a very stimulating perspective.

## Relevant publications

[210] H. Price, Y. Chong, A. Khanikaev, H. Schomerus, L. J. Maczewsky, M. Kremer, M. Heinrich, A. Szameit, O. Zilberberg, Y. Yang, B. Zhang, A. Alù, R. Thomale, I. Carusotto, P. St-Jean, A. Amo, A. Dutt, L. Yuan, S. Fan, X. Yin, Ch. Peng, T. Ozawa, and A. Blanco-Redondo. *Roadmap on topological photonics*. *J. Phys. Photonics* **4**, 032501 (2022).

# References

- [1] K. v. Klitzing, G. Dorda, and M. Pepper. New Method for High-Accuracy Determination of the Fine-Structure Constant Based on Quantized Hall Resistance. *Phys. Rev. Lett.*, 45(6):494–497, August 1980.
- [2] D. Thouless, M. Kohmoto, M. Nightingale, and M. den Nijs. Quantized Hall Conductance in a Two-Dimensional Periodic Potential. *Physical Review Letters*, 49(6):405–408, August 1982.
- [3] Yasuhiro Hatsugai. Chern number and edge states in the integer quantum Hall effect. *Physical Review Letters*, 71(22):3697–3700, November 1993. Publisher: American Physical Society.
- [4] Xiao-Liang Qi, Yong-Shi Wu, and Shou-Cheng Zhang. General theorem relating the bulk topological number to edge states in two-dimensional insulators. *Phys. Rev. B*, 74(4):045125, July 2006.
- [5] F. D. M. Haldane. Model for a Quantum Hall Effect without Landau Levels: Condensed-Matter Realization of the "Parity Anomaly". *Physical Review Letters*, 61(18):2015–2018, October 1988. Publisher: American Physical Society.
- [6] D. J. Thouless. Quantization of particle transport. *Physical Review B*, 27(10):6083–6087, 1983. Publisher: American Physical Society.
- [7] B. Andrei Bernevig, Taylor L. Hughes, and Shou-Cheng Zhang. Quantum Spin Hall Effect and Topological Phase Transition in HgTe Quantum Wells. *Science (New York, N.Y.)*, 314:1757, 2006.
- [8] C. L. Kane and E. J. Mele.  $Z_2$  Topological Order and the Quantum Spin Hall Effect. *Phys. Rev. Lett.*, 95(14):146802, September 2005.
- [9] Markus König, Steffen Wiedmann, Christoph Bröne, Andreas Roth, Hartmut Buhmann, Laurens W Molenkamp, Xiao-Liang Qi, and Shou-Cheng Zhang. Quantum Spin Hall Insulator State in HgTe Quantum Wells. *Science (New York, N.Y.)*, 318(5851):766–770, 2007.
- [10] Andreas Schnyder, Shinsei Ryu, Akira Furusaki, and Andreas Ludwig. Classification of topological insulators and superconductors in three spatial dimensions. *Physical Review B*, 78(19):195125, November 2008.
- [11] Takuya Kitagawa, Erez Berg, Mark Rudner, and Eugene Demler. Topological characterization of periodically driven quantum systems. *Phys. Rev. B*, 82(23):235114, December 2010.

- [12] Takuya Kitagawa, Matthew A Broome, Alessandro Fedrizzi, Mark S Rudner, Erez Berg, Ivan Kassal, Alan Aspuru-Guzik, Eugene Demler, and Andrew G White. Observation of topologically protected bound states in photonic quantum walks. *Nat. Commun.*, 3:882, 2012.
- [13] Mark S Rudner, Netanel H Lindner, Erez Berg, and Michael Levin. Anomalous Edge States and the Bulk-Edge Correspondence for Periodically Driven Two-Dimensional Systems. *Physical Review X*, 3(3):31005, July 2013. Publisher: American Physical Society.
- [14] Ling Lu, Zhiyu Wang, Dexin Ye, Lixin Ran, Liang Fu, John D. Joannopoulos, and Marin Soljačić. Experimental observation of Weyl points. *Science (New York, N.Y.)*, 349(6248), 2015.
- [15] Wladimir A Benalcazar, B Andrei Bernevig, and Taylor L Hughes. Quantized electric multipole insulators. *Science*, 357(6346):61 LP – 66, July 2017.
- [16] Zongping Gong, Yuto Ashida, Kohei Kawabata, Kazuaki Takasan, Sho Higashikawa, and Masahito Ueda. Topological Phases of Non-Hermitian Systems. *Physical Review X*, 8(3):31079, September 2018. Publisher: American Physical Society.
- [17] Jennifer Cano, Barry Bradlyn, Zhijun Wang, L. Elcoro, M. G. Vergniory, C. Felser, M. I. Aroyo, and B. Andrei Bernevig. Topology of Disconnected Elementary Band Representations. *Phys. Rev. Lett.*, 120(26):266401, June 2018.
- [18] Shinsei Ryu and Yasuhiro Hatsugai. Topological origin of zero-energy edge states in particle-hole symmetric systems. *Physical review letters*, 89(7):077002, 2002. arXiv: cond-mat/0112197 ISBN: 0031-9007 (Print)\n0031-9007 (Linking).
- [19] P. Delplace, D. Ullmo, and G. Montambaux. Zak phase and the existence of edge states in graphene. *Physical Review B*, 84(19):195452, November 2011.
- [20] M Hafezi, S Mittal, J Fan, A Migdall, and J M Taylor. Imaging topological edge states in silicon photonics. *Nat. Photon.*, 7(12):1001–1005, 2013.
- [21] Mikael C Rechtsman, Julia M Zeuner, Yonatan Plotnik, Yaakov Lumer, Daniel Podolsky, Felix Dreisow, Stefan Nolte, Mordechai Segev, and Alexander Szameit. Photonic Floquet topological insulators. *Nature*, 496(7444):196–200, 2013.
- [22] Babak Bahari, Abdoulaye Ndao, Felipe Vallini, Abdelkrim El Amili, Yeshaiahu Fainman, and Boubacar Kanté. Nonreciprocal lasing in topological cavities of arbitrary geometries. *Science*, 358(6363):636–640, 2017.
- [23] F. D. M. Haldane and S. Raghu. Possible Realization of Directional Optical Waveguides in Photonic Crystals with Broken Time-Reversal Symmetry. *Physical Review Letters*, 100(1):013904, January 2008. Publisher: American Physical Society.
- [24] Zheng Wang, Yidong Chong, J. D. Joannopoulos, and Marin Soljačić. Observation of unidirectional backscattering-immune topological electromagnetic states. *Nature*, 461(7265):772–775, October 2009. Publisher: Nature Publishing Group.

- [25] Fengcheng Wu, Fanyao Qu, and A. H. MacDonald. Exciton band structure of monolayer MoS<sub>2</sub>. *arXiv:1501.02273*, page 9, January 2015. arXiv: 1501.02273 Genre: Mesoscale and Nanoscale Physics.
- [26] Lukas J Maczewsky, Julia M Zeuner, Stefan Nolte, and Alexander Szameit. Observation of photonic anomalous Floquet topological insulators. *Nature Communications*, 8:13756, January 2017.
- [27] Seabrata Mukherjee, Alexander Spracklen, Manuel Valiente, Erika Andersson, Patrik Öhberg, Nathan Goldman, and Robert R. Thomson. Experimental observation of anomalous topological edge modes in a slowly driven photonic lattice. *Nature Communications*, 8:13918, January 2017. Publisher: Nature Publishing Group.
- [28] Jiho Noh, Sheng Huang, Daniel Leykam, Y. D. Chong, Kevin P. Chen, and Mikael C. Rechtsman. Experimental observation of optical Weyl points and Fermi arc-like surface states. *Nature Physics*, 13:611–617, 2017.
- [29] Ling Lu, John D. Joannopoulos, and Marin Soljačić. Topological photonics. *Nature Photonics*, 8(11):821–829, October 2014. Publisher: Nature Publishing Group, a division of Macmillan Publishers Limited. All Rights Reserved.
- [30] Tomoki Ozawa, Hannah M Price, Alberto Amo, Nathan Goldman, Mohammad Hafezi, Ling Lu, Mikael C Rechtsman, David Schuster, Jonathan Simon, Oded Zilberberg, and Iacopo Carusotto. Topological photonics. *Reviews of Modern Physics*, 91(1):15006, March 2019. Publisher: American Physical Society.
- [31] P St-Jean, V Goblot, E Galopin, A Lemaître, T Ozawa, L Le Gratiet, I Sagnes, J Bloch, and A Amo. Lasing in topological edge states of a one-dimensional lattice. *Nature Photonics*, 11(10):651–656, 2017.
- [32] Miguel A Bandres, Steffen Wittek, Gal Harari, Midya Parto, Jinhan Ren, Mordechai Segev, Demetrios N Christodoulides, and Mercedeh Khajavikhan. Topological insulator laser: Experiments. *Science*, 359(6381):aar4005, March 2018.
- [33] S Klemmt, T H Harder, O A Egorov, K Winkler, R Ge, M A Bandres, M Emmerling, L Worschech, T C H Liew, M Segev, C Schneider, and S Höfling. Exciton-polariton topological insulator. *Nature*, 562(7728):552–556, 2018.
- [34] Yihao Yang, Yuichiro Yamagami, Xiongbin Yu, Prakash Pitchappa, Julian Webber, Baile Zhang, Masayuki Fujita, Tadao Nagatsuma, and Ranjan Singh. Terahertz topological photonics for on-chip communication. *Nature Photonics*, 14(7):446–451, 2020.
- [35] Yongquan Zeng, Udvas Chattopadhyay, Bofeng Zhu, Bo Qiang, Jinghao Li, Yuhao Jin, Lianhe Li, Alexander Giles Davies, Edmund Harold Linfield, Baile Zhang, Yidong Chong, and Qi Jie Wang. Electrically pumped topological laser with valley edge modes. *Nature*, 578(7794):246–250, 2020.
- [36] Babak Bahari, Liyi Hsu, Si Hui Pan, Daryl Preece, Abdoulaye Ndao, Abdelkrim El Amili, Yashaiahu Fainman, and Boubacar Kanté. Photonic quantum Hall effect and multiplexed light sources of large orbital angular momenta. *Nat. Phys.*, 17(6):700–703, June 2021.

- [37] Charles Poli, Matthieu Bellec, Ulrich Kuhl, Fabrice Mortessagne, and Henning Schomerus. Selective enhancement of topologically induced interface states in a dielectric resonator chain. *Nature Communications*, 6:6710, April 2015. Publisher: Nature Publishing Group.
- [38] Julia M. Zeuner, Mikael C. Rechtsman, Yonatan Plotnik, Yaakov Lumer, Stefan Nolte, Mark S. Rudner, Mordechai Segev, and Alexander Szameit. Observation of a Topological Transition in the Bulk of a Non-Hermitian System. *Physical Review Letters*, 115(4):040402, July 2015. Publisher: American Physical Society.
- [39] Yaacov E. Kraus, Yoav Lahini, Zohar Ringel, Mor Verbin, and Oded Zilberberg. Topological States and Adiabatic Pumping in Quasicrystals. *Physical Review Letters*, 109(10):106402, September 2012.
- [40] Sabyasachi Barik, Aziz Karasahin, Christopher Flower, Tao Cai, Hirokazu Miyake, Wade DeGottardi, Mohammad Hafezi, and Edo Waks. A topological quantum optics interface. *Science*, 359(6376):666–668, February 2018.
- [41] Andrea Blanco-Redondo, Bryn Bell, Dikla Oren, Benjamin J Eggleton, and Mordechai Segev. Topological protection of biphoton states. *Science (New York, N.Y.)*, 362(6414):568 LP – 571, November 2018.
- [42] Sebastian Weidemann, Mark Kremer, Tobias Helbig, Tobias Hofmann, Alexander Stegmaier, Martin Greiter, Ronny Thomale, and Alexander Szameit. Topological funneling of light. *Science (New York, N.Y.)*, 368(6488):311–314, April 2020.
- [43] Kai Wang, Avik Dutt, Ki Youl Yang, Casey C. Wojcik, Jelena Vučković, and Shanhui Fan. Generating arbitrary topological windings of a non-Hermitian band. *Science*, 371(6535):1240–1245, March 2021.
- [44] Kai Wang, Avik Dutt, Charles C. Wojcik, and Shanhui Fan. Topological complex-energy braiding of non-Hermitian bands. *Nature*, 598(7879):59–64, October 2021.
- [45] Sunil Mittal, Sriram Ganeshan, Jingyun Fan, Abolhassan Vaezi, and Mohammad Hafezi. Measurement of topological invariants in a 2D photonic system. *Nature Photonics*, 10(3):180–183, February 2016. Publisher: Nature Publishing Group.
- [46] Martin Wimmer, Hannah M Price, Iacopo Carusotto, and Ulf Peschel. Experimental measurement of the Berry curvature from anomalous transport. *Nature Physics*, 13:545, February 2017. Publisher: Nature Publishing Group.
- [47] Filippo Cardano, Alessio D’Errico, Alexandre Dauphin, Maria Maffei, Bruno Piccirillo, Corrado de Lisio, Giulio De Filippis, Vittorio Cataudella, Enrico Santamato, Lorenzo Marrucci, Maciej Lewenstein, and Pietro Massignan. Detection of Zak phases and topological invariants in a chiral quantum walk of twisted photons. *Nature Communications*, 8:15516, June 2017. Publisher: Nature Publishing Group.
- [48] A Gianfrate, O Bleu, L Dominici, V Ardizzone, M De Giorgi, D Ballarini, G Lerario, K W West, L N Pfeiffer, D D Solnyshkov, D Sanvitto, and G Malpuech. Measurement of the quantum geometric tensor and of the anomalous Hall drift. *Nature*, 578(7795):381–385, 2020.

- [49] P. St-Jean, A. Dauphin, P. Massignan, B. Real, O. Jamadi, M. Milicevic, A. Lemaître, A. Harouri, L. Le Gratiet, I. Sagnes, S. Ravets, J. Bloch, and A. Amo. Measuring Topological Invariants in a Polaritonic Analog of Graphene. *Phys. Rev. Lett.*, 126(12):127403, March 2021.
- [50] Clément Dutreix, Matthieu Bellec, Pierre Delpace, and Fabrice Mortessagne. Wavefront dislocations reveal the topology of quasi-1D photonic insulators. *Nat Commun*, 12(1):3571, December 2021.
- [51] A. Bisianov, M. Wimmer, U. Peschel, and O. A. Egorov. Stability of topologically protected edge states in nonlinear fiber loops. *Phys. Rev. A*, 100(6):063830, December 2019.
- [52] Shiqi Xia, Dario Jukić, Nan Wang, Daria Smirnova, Lev Smirnov, Liqin Tang, Daohong Song, Alexander Szameit, Daniel Leykam, Jingjun Xu, Zhigang Chen, and Hrvoje Buljan. Nontrivial coupling of light into a defect: the interplay of nonlinearity and topology. *Light Sci Appl*, 9(1):147, December 2020.
- [53] Lukas J. Maczewsky, Matthias Heinrich, Mark Kremer, Sergey K. Ivanov, Max Ehrhardt, Franklin Martinez, Yaroslav V. Kartashov, Vladimir V. Konotop, Lluís Torner, Dieter Bauer, and Alexander Szameit. Nonlinearity-induced photonic topological insulator. *Science*, 370(6517):701–704, November 2020.
- [54] Seabrata Mukherjee and Mikael C Rechtsman. Observation of Floquet solitons in a topological bandgap. *Science*, 368(6493):856 LP – 859, May 2020.
- [55] Seabrata Mukherjee and Mikael C. Rechtsman. Observation of Unidirectional Solitonlike Edge States in Nonlinear Floquet Topological Insulators. *Phys. Rev. X*, 11(4):041057, December 2021.
- [56] Mohammad Hafezi, Eugene A Demler, Mikhail D Lukin, and Jacob M Taylor. Robust optical delay lines with topological protection. *Nature Phys.*, 7(11):907–912, 2011.
- [57] Julian Webber, Yuichiro Yamagami, Guillaume Ducournau, Pascal Szriftgiser, Kei Iyoda, Masayuki Fujita, Tadao Nagatsuma, and Ranjan Singh. Terahertz Band Communications With Topological Valley Photonic Crystal Waveguide. *J. Lightwave Technol.*, 39(24):7609–7620, December 2021.
- [58] C Schneider, K Winkler, M D Fraser, M Kamp, Y Yamamoto, E A Ostrovskaya, and S Höfling. Exciton-polariton trapping and potential landscape engineering. *Reports on Progress in Physics*, 80(1):016503, January 2017. Publisher: IOP Publishing.
- [59] Iacopo Carusotto and Cristiano Ciuti. Quantum fluids of light. *Reviews of Modern Physics*, 85(1):299–366, February 2013. Publisher: American Physical Society.
- [60] Giovanna Panzarini, Lucio Claudio Andreani, A Armitage, D Baxter, M S Skolnick, V N Astratov, J S Roberts, Alexey V Kavokin, Maria R Vladimirova, and M A Kaliteevski. Exciton-light coupling in single and coupled semiconductor microcavities: Polariton dispersion and polarization splitting. *Phys. Rev. B*, 59(7):5082–5089, 1999.
- [61] Alexey Kavokin, Guillaume Malpuech, and Mikhail Glazov. Optical Spin Hall Effect. *Phys. Rev. Lett.*, 95(13):136601, 2005.

- [62] A. V. Nalitov, D. D. Solnyshkov, and G. Malpuech. Polariton Z Topological Insulator. *Physical Review Letters*, 114(11):116401, March 2015.
- [63] Torsten Karzig, Charles-Edouard Bardyn, Netanel H. Lindner, and Gil Refael. Topological Polaritons. *Physical Review X*, 5(3):031001, July 2015.
- [64] C Ciuti, V Savona, C Piermarocchi, A Quattropani, and P Schwendimann. Role of the exchange of carriers in elastic exciton-exciton scattering in quantum wells. *Phys. Rev. B*, 58(12):7926–7933, 1998.
- [65] P. G. Lagoudakis, P. G. Savvidis, J. J. Baumberg, D. M. Whittaker, P. R. Eastham, M. S. Skolnick, and J. S. Roberts. Stimulated spin dynamics of polaritons in semiconductor microcavities. *Phys. Rev. B*, 65(16):161310, April 2002.
- [66] I. Shelykh, G. Malpuech, K. V. Kavokin, A. V. Kavokin, and P. Bigenwald. Spin dynamics of interacting exciton polaritons in microcavities. *Phys. Rev. B*, 70(11):115301, September 2004.
- [67] M. Vladimirova, S. Cronenberger, D. Scalbert, K. V. Kavokin, A. Miard, A. Lemaître, J. Bloch, D. Solnyshkov, G. Malpuech, and A. V. Kavokin. Polariton-polariton interaction constants in microcavities. *Phys. Rev. B*, 82(7):075301, August 2010.
- [68] P. Cilibrizzi, H. Sigurdsson, T. C. H. Liew, H. Ohadi, S. Wilkinson, A. Askitopoulos, I. A. Shelykh, and P. G. Lagoudakis. Polariton spin whirls. *Physical Review B*, 92(15):155308, October 2015.
- [69] L. Pickup, K. Kalinin, A. Askitopoulos, Z. Hatzopoulos, P. G. Savvidis, N. G. Berloff, and P. G. Lagoudakis. Optical Bistability under Nonresonant Excitation in Spinor Polariton Condensates. *Phys. Rev. Lett.*, 120(22):225301, May 2018.
- [70] C. E. Whittaker, D. R. Gulevich, D. Biegańska, B. Royall, E. Clarke, M. S. Skolnick, I. A. Shelykh, and D. N. Krizhanovskii. Optical and magnetic control of orbital flat bands in a polariton Lieb lattice. *Phys. Rev. A*, 104(6):063505, December 2021.
- [71] R M Stevenson, V N Astratov, M S Skolnick, D M Whittaker, M Emam-Ismael, A I Tartakovskii, P G Savvidis, J J Baumberg, and J S Roberts. Continuous Wave Observation of Massive Polariton Redistribution by Stimulated Scattering in Semiconductor Microcavities. *Phys. Rev. Lett.*, 85(17):3680–3683, 2000.
- [72] P G Savvidis, J J Baumberg, R M Stevenson, M S Skolnick, D M Whittaker, and J S Roberts. Angle-Resonant Stimulated Polariton Amplifier. *Phys. Rev. Lett.*, 84(7):1547, 2000.
- [73] J Kasprzak, M Richard, S Kundermann, A Baas, P Jeambrun, J M J Keeling, F M Marchetti, M H Szymanska, R Andre, J L Staehli, V Savona, P B Littlewood, B Deveaud, and Le Si; Dang. Bose-Einstein condensation of exciton polaritons. *Nature*, 443(7110):409–414, 2006.
- [74] R Balili, V Hartwell, D Snoke, L Pfeiffer, and K West. Bose-Einstein Condensation of Microcavity Polaritons in a Trap. *Science*, 316(5827):1007–1010, 2007.

- [75] Alberto Amo, Jérôme Lefrère, Simon Pigeon, Claire Adrados, Cristiano Ciuti, Iacopo Carusotto, Romuald Houdré, Elisabeth Giacobino, and Alberto Bramati. Superfluidity of polaritons in semiconductor microcavities. *Nature Physics*, 5:805, September 2009. Publisher: Nature Publishing Group.
- [76] V. Kohnle, Y. Léger, M. Wouters, M. Richard, M. T. Portella-Oberli, and B. Deveaud-Plédran. From Single Particle to Superfluid Excitations in a Dissipative Polariton Gas. *Phys. Rev. Lett.*, 106(25):255302, June 2011.
- [77] Petr Stepanov, Ivan Amelio, Jean-Guy Rousset, Jacqueline Bloch, Aristide Lemaître, Alberto Amo, Anna Minguzzi, Iacopo Carusotto, and Maxime Richard. Dispersion relation of the collective excitations in a resonantly driven polariton fluid. *Nat Commun*, 10(1):3869, December 2019.
- [78] A Amo, S Pigeon, D Sanvitto, V G Sala, R Hivet, I Carusotto, F Pisanello, G Leménager, R Houdré, E Giacobino, C Ciuti, and A Bramati. Polariton superfluids reveal quantum hydrodynamic solitons. *Science*, 332(6034):1167–1170, 2011. Publisher: Laboratoire Kastler Brossel, Université Pierre et Marie Curie-Paris 6, École Normale Supérieure et CNRS, UPMC Case 74, 4 place Jussieu, 75005 Paris, France. alberto.amo@lpn.cnrs.fr.
- [79] R. Hivet, H. Flayac, D. D. Solnyshkov, D. Tanese, T. Boulier, D. Andreoli, E. Giacobino, J. Bloch, A. Bramati, G. Malpuech, and A. Amo. Half-solitons in a polariton quantum fluid behave like magnetic monopoles. *Nature Physics*, 8(10):724–728, 2012.
- [80] G Grosso, G Nardin, F Morier-Genoud, Y Léger, and B Deveaud-Plédran. Soliton Instabilities and Vortex Street Formation in a Polariton Quantum Fluid. *Phys. Rev. Lett.*, 107(24):245301, 2011.
- [81] M Sich, D N Krizhanovskii, M S Skolnick, A V Gorbach, R Hartley, D V Skryabin, E A Cerda-Méndez, K Biermann, R Hey, and P V Santos. Observation of bright polariton solitons in a semiconductor microcavity. *Nature Photonics*, 6:50–55, November 2011. Publisher: Nature Publishing Group.
- [82] C Weisbuch, M Nishioka, A Ishikawa, and Y Arakawa. Observation of the coupled exciton-photon mode splitting in a semiconductor quantum microcavity. *Phys. Rev. Lett.*, 69(23):3314–3317, 1992.
- [83] Le Si Dang, D. Heger, R. André, F. Bœuf, and R. Romestain. Stimulation of Polariton Photoluminescence in Semiconductor Microcavity. *Phys. Rev. Lett.*, 81(18):3920–3923, November 1998.
- [84] G Christmann, R Butte, E Feltin, J-F. Carlin, and N Grandjean. Room temperature polariton lasing in a GaN/AlGaIn multiple quantum well microcavity. *Appl. Phys. Lett.*, 93:51102, 2008.
- [85] R. Schmidt-Grund, B. Rheinländer, C. Czekalla, G. Benndorf, H. Hochmut, A. Rahm, M. Lorenz, and M. Grundmann. ZnO based planar and micropillar resonators. *Superlattices and Microstructures*, 41(5-6):360–363, May 2007.

- [86] Feng Li, L. Orosz, O. Kamoun, S. Bouchoule, C. Brimont, P. Disseix, T. Guillet, X. Lafosse, M. Leroux, J. Leymarie, M. Mexis, M. Mihailovic, G. Patriarche, F. Réveret, D. Solnyshkov, J. Zuniga-Perez, and G. Malpuech. From Excitonic to Photonic Polariton Condensate in a ZnO-Based Microcavity. *Phys. Rev. Lett.*, 110(19):196406, May 2013.
- [87] S Kena-Cohen and S R Forrest. Room-temperature polariton lasing in an organic single-crystal microcavity. *Nature Phot.*, 4(6):371–375, 2010.
- [88] Johannes D Plumhof, Thilo Stöferle, Lijian Mai, Ullrich Scherf, and Rainer F Mahrt. Room-temperature Bose–Einstein condensation of cavity exciton–polaritons in a polymer. *Nature Materials*, 13(3):247–252, 2014.
- [89] Xiaoze Liu, Tal Galfsky, Zheng Sun, Fengnian Xia, Erh-chen Lin, Yi-Hsien Lee, Stéphane Kéna-Cohen, and Vinod M Menon. Strong light–matter coupling in two-dimensional atomic crystals. *Nature Photonics*, 9(1):30–34, 2015.
- [90] S Dufferwiel, S Schwarz, F Withers, A A P Trichet, F Li, M Sich, O Del Pozo-Zamudio, C Clark, A Nalitov, D D Solnyshkov, G Malpuech, K S Novoselov, J M Smith, M S Skolnick, D N Krizhanovskii, and A I Tartakovskii. Exciton–polaritons in van der Waals heterostructures embedded in tunable microcavities. *Nature Communications*, 6(1):8579, 2015.
- [91] David M. Coles, Yanshen Yang, Yaya Wang, Richard T. Grant, Robert A. Taylor, Semion K. Saikin, Alán Aspuru-Guzik, David G. Lidzey, Joseph Kuo-Hsiang Tang, and Jason M. Smith. Strong coupling between chlorosomes of photosynthetic bacteria and a confined optical cavity mode. *Nat Commun*, 5(1):5561, December 2014.
- [92] G G Paschos, N Somaschi, S I Tsintzos, D Coles, J L Bricks, Z Hatzopoulos, D G Lidzey, P G Lagoudakis, and P G Savvidis. Hybrid organic-inorganic polariton laser. *Scientific Reports*, 7(1):11377, 2017.
- [93] Max Waldherr, Nils Lundt, Martin Klaas, Simon Betzold, Matthias Wurdack, Vasilij Baumann, Eliezer Estrecho, Anton Nalitov, Evgenia Cherotchenko, Hui Cai, Elena A Ostrovskaya, Alexey V Kavokin, Sefaattin Tongay, Sebastian Klemmt, Sven Höfling, and Christian Schneider. Observation of bosonic condensation in a hybrid monolayer MoSe<sub>2</sub>-GaAs microcavity. *Nature Communications*, 9(1):3286, 2018.
- [94] Yongbao Sun, Patrick Wen, Yoseob Yoon, Gangqiang Liu, Mark Steger, Loren N Pfeiffer, Ken West, David W Snoke, and Keith A Nelson. Bose-Einstein Condensation of Long-Lifetime Polaritons in Thermal Equilibrium. *Physical Review Letters*, 118(1):16602, January 2017. Publisher: American Physical Society.
- [95] M. Bayer, T. Gutbrod, J. P. Reithmaier, A. Forchel, T. L. Reinecke, P. A. Knipp, A. A. Dremin, and V. D. Kulakovskii. Optical Modes in Photonic Molecules. *Physical Review Letters*, 81(12):2582–2585, September 1998.
- [96] M. Bayer, T. Gutbrod, A. Forchel, T. L. Reinecke, P. A. Knipp, R. Werner, and J. P. Reithmaier. Optical Demonstration of a Crystal Band Structure Formation. *Physical Review Letters*, 83(25):5374–5377, December 1999. Publisher: American Physical Society.

- [97] Marta Galbiati, Lydie Ferrier, Dmitry D Solnyshkov, Dimitrii Tanese, Esther Wertz, Alberto Amo, Marco Abbarchi, Pascale Senellart, Isabelle Sagnes, Aristide Lemaître, Elisabeth Galopin, Guillaume Malpuech, and Jacqueline Bloch. Polariton Condensation in Photonic Molecules. *Phys. Rev. Lett.*, 108(12):126403, 2012.
- [98] S.; de Vasconcellos, A Calvar, A Dousse, J Suffczynski, N Dupuis, A Lemaître, I Sagnes, J Bloch, P Voisin, and P Senellart. Spatial, spectral, and polarization properties of coupled micropillar cavities. *Appl. Phys. Lett.*, 99(10):101103, 2011.
- [99] Alberto Amo and Jacqueline Bloch. Exciton-polaritons in lattices: A non-linear photonic simulator. *Comptes Rendus Physique*, 17(8):934–945, 2016.
- [100] Franco Mangussi, Marijana Milićević, Isabelle Sagnes, Luc Le Gratiet, Abdelmounaim Harouri, Aristide Lemaître, Jacqueline Bloch, Alberto Amo, and Gonzalo Usaj. Multi-orbital tight binding model for cavity-polariton lattices. *Journal of Physics: Condensed Matter*, 32(31):315402, 2020. Publisher: IOP Publishing.
- [101] Thibaut Jacqmin, Iacopo Carusotto, Isabelle Sagnes, Marco Abbarchi, Dmitry Solnyshkov, Guillaume Malpuech, Elisabeth Galopin, Aristide Lemaître, Jacqueline Bloch, and Alberto Amo. Direct Observation of Dirac Cones and a Flatband in a Honeycomb Lattice for Polaritons. *Phys. Rev. Lett.*, 112(11):116402, 2014.
- [102] Dmitry D. Solnyshkov, Guillaume Malpuech, Philippe St-Jean, Sylvain Ravets, Jacqueline Bloch, and Alberto Amo. Microcavity polaritons for topological photonics. *Opt. Mater. Express*, 11(4):1119, April 2021.
- [103] K. Y. Bliokh, F. J. Rodríguez-Fortuño, F. Nori, and A. V. Zayats. Spin-orbit interactions of light. *Nat. Photon.*, 9(12):796–808, November 2015. Publisher: Nature Publishing Group ISBN: doi:10.1038/nphoton.2015.201.
- [104] W Langbein, I Shelykh, D Solnyshkov, G Malpuech, Yu. Rubo, and A Kavokin. Polarization beats in ballistic propagation of exciton-polaritons in microcavities. *Phys. Rev. B*, 75(7):75323, 2007.
- [105] C. Leyder, M. Romanelli, J. Ph. Karr, E. Giacobino, T. C. H. Liew, M. M. Glazov, A. V. Kavokin, G. Malpuech, and A. Bramati. Observation of the optical spin Hall effect. *Nature Physics*, 3(9):628–631, September 2007. Publisher: Nature Publishing Group.
- [106] A Amo, T C H Liew, C Adrados, E Giacobino, A V Kavokin, and A Bramati. Anisotropic optical spin Hall effect in semiconductor microcavities. *Phys. Rev. B*, 80(16):165325, 2009.
- [107] E Kammann, T C H Liew, H Ohadi, P Cilibrizzi, P Tsotsis, Z Hatzopoulos, P G Savvidis, A V Kavokin, and P G Lagoudakis. Nonlinear Optical Spin Hall Effect and Long-Range Spin Transport in Polariton Lasers. *Phys. Rev. Lett.*, 109(3):36404, 2012.
- [108] V. G. Sala, D. D. Solnyshkov, I. Carusotto, T. Jacqmin, A. Lemaître, H. Terças, A. Nalitov, M. Abbarchi, E. Galopin, I. Sagnes, J. Bloch, G. Malpuech, and A. Amo. Spin-Orbit Coupling for Photons and Polaritons in Microstructures. *Physical Review X*, 5(1):011034, March 2015.

- [109] A V Nalitov, G Malpuech, H Terças, and D D Solnyshkov. Spin-Orbit Coupling and the Optical Spin Hall Effect in Photonic Graphene. *Physical review letters*, 114(2):026803, January 2015. Publisher: American Physical Society.
- [110] Yaroslav V. Kartashov and Dmitry V. Skryabin. Modulational instability and solitary waves in polariton topological insulators. *Optica*, 3(11):1228, November 2016. Publisher: Optical Society of America.
- [111] Yaroslav V. Kartashov and Dmitry V. Skryabin. Two-dimensional lattice solitons in polariton condensates with spin-orbit coupling. *Optics Letters*, 41(21):5043, November 2016. Publisher: Optical Society of America.
- [112] S Klemmt, T H Harder, O A Egorov, K Winkler, H Suchomel, J Beierlein, M Emmerling, C Schneider, and S Höfling. Polariton condensation in S- and P-flatbands in a two-dimensional Lieb lattice. *Applied Physics Letters*, 111(23):231102, December 2017. Publisher: American Institute of Physics.
- [113] C E Whittaker, E Cancellieri, P M Walker, D R Gulevich, H Schomerus, D Vaitiekus, B Royall, D M Whittaker, E Clarke, I V Iorsh, I A Shelykh, M S Skolnick, and D N Krizhanovskii. Exciton Polaritons in a Two-Dimensional Lieb Lattice with Spin-Orbit Coupling. *Phys. Rev. Lett.*, 120(9):97401, March 2018. Publisher: American Physical Society.
- [114] C. E. Whittaker, T. Dowling, A. V. Nalitov, A. V. Yulin, B. Royall, E. Clarke, M. S. Skolnick, I. A. Shelykh, and D. N. Krizhanovskii. Optical analogue of Dresselhaus spin-orbit interaction in photonic graphene. *Nat. Photonics*, November 2020.
- [115] N. Carlon Zambon, P. St-Jean, M. Milićević, A. Lemaître, A. Harouri, L. Le Gratiet, O. Bleu, D.D. Solnyshkov, G. Malpuech, I. Sagnes, S. Ravets, A. Amo, and J. Bloch. Optically controlling the emission chirality of microlasers. *Nature Photonics*, 13(4):283–288, 2019.
- [116] N Carlon Zambon, P St-Jean, A Lemaître, A Harouri, L Le Gratiet, I Sagnes, S Ravets, A Amo, and J Bloch. Orbital angular momentum bistability in a microlaser. *Optics Letters*, 44(18):4531–4534, 2019. Publisher: OSA.
- [117] A V Larionov, V D Kulakovskii, S Höfling, C Schneider, L Worschech, and A Forchel. Polarized Nonequilibrium Bose-Einstein Condensates of Spinor Exciton Polaritons in a Magnetic Field. *Phys. Rev. Lett.*, 105(25):256401, 2010. Publisher: American Physical Society.
- [118] P. Walker, T. C.H. Liew, D. Sarkar, M. Durska, A. P.D. Love, M. S. Skolnick, J. S. Roberts, I. A. Shelykh, A. V. Kavokin, and D. N. Krizhanovskii. Suppression of Zeeman splitting of the energy levels of exciton-polariton condensates in semiconductor microcavities in an external magnetic field. *Physical Review Letters*, 106(25):257401, June 2011. Publisher: American Physical Society.
- [119] B Piętko, D Zygmunt, M Król, M R Molas, A A L Nicolet, F Morier-Genoud, J Szczytko, J Łusakowski, P Zięba, I Tralle, P Stępnicki, M Matuszewski, M Potemski, and B Deveaud. Magnetic field tuning of exciton-polaritons in a semiconductor microcavity. *Physical Review B*, 91(7):75309, February 2015. Publisher: American Physical Society.

- [120] C. Sturm, D. Solnyshkov, O. Krebs, A. Lemaître, I. Sagnes, E. Galopin, A. Amo, G. Malpuech, and J. Bloch. Nonequilibrium polariton condensate in a magnetic field. *Physical Review B - Condensed Matter and Materials Physics*, 91(15):155130, April 2015.
- [121] D Sarkar, S S Gavrilov, M Sich, J H Quilter, R A Bradley, N A Gippius, K Guda, V D Kulakovskii, M S Skolnick, and D N Krizhanovskii. Polarization Bistability and Resultant Spin Rings in Semiconductor Microcavities. *Phys. Rev. Lett.*, 105(21):216402, 2010.
- [122] C Adrados, A Amo, T C H Liew, R Hivet, R Houdré, E Giacobino, A V Kavokin, and A Bramati. Spin Rings in Bistable Planar Semiconductor Microcavities. *Phys. Rev. Lett.*, 105(21):216403, 2010.
- [123] M. Sich, F. Fras, J. K. Chana, M. S. Skolnick, D. N. Krizhanovskii, A. V. Gorbach, R. Hartley, D. V. Skryabin, S. S. Gavrilov, E. A. Cerda-Méndez, K. Biermann, R. Hey, and P. V. Santos. Effects of Spin-Dependent Interactions on Polarization of Bright Polariton Solitons. *Phys. Rev. Lett.*, 112(4):046403, January 2014.
- [124] N. Takemura, S. Trebaol, M. Wouters, M. T. Portella-Oberli, and B. Deveaud. Polaronic Feshbach resonance. *Nat. Phys.*, 10(7):500–504, June 2014. Publisher: Nature Publishing Group.
- [125] I. Gnusov, H. Sigurdsson, S. Baryshev, T. Ermatov, A. Askitopoulos, and P. G. Lagoudakis. Optical orientation, polarization pinning, and depolarization dynamics in optically confined polariton condensates. *Phys. Rev. B*, 102(12):125419, September 2020.
- [126] B. Real, N. Carlon Zambon, P. St-Jean, I. Sagnes, A. Lemaître, L. Le Gratiet, A. Harouri, S. Ravets, J. Bloch, and A. Amo. Chiral emission induced by optical Zeeman effect in polariton micropillars. *Phys. Rev. Research*, 3(4):043161, December 2021.
- [127] S Dufferwiel, Feng Li, E Cancellieri, L Giriunas, A A P Trichet, D M Whittaker, P M Walker, F Fras, E Clarke, J M Smith, M S Skolnick, and D N Krizhanovskii. Spin Textures of Exciton-Polaritons in a Tunable Microcavity with Large TE-TM Splitting. *Physical review letters*, 115(24):246401, December 2015. Publisher: American Physical Society.
- [128] Charles-Edouard Bardyn, Torsten Karzig, Gil Refael, and Timothy C H Liew. Topological Polaritons and Excitons in Garden Variety Systems. *Phys. Rev. B*, 91:161413(R), 2015.
- [129] O. Bleu, D. D. Solnyshkov, and G. Malpuech. Interacting quantum fluid in a polariton Chern insulator. *Physical Review B*, 93(8):085438, February 2016. Publisher: American Physical Society.
- [130] O Bleu, D D Solnyshkov, and G Malpuech. Photonic versus electronic quantum anomalous Hall effect. *Physical Review B*, 95(11):115415, March 2017. Publisher: American Physical Society.

- [131] O Bleu, G Malpuech, and D D Solnyshkov. Robust quantum valley Hall effect for vortices in an interacting bosonic quantum fluid. *Nature Communications*, 9(1):3991, 2018.
- [132] Charles-Edouard Bardyn, Torsten Karzig, Gil Refael, and Timothy C. H. Liew. Chiral Bogoliubov excitations in nonlinear bosonic systems. *Physical Review B*, 93(2):020502, January 2016. Publisher: American Physical Society.
- [133] Yaroslav V. Kartashov and Dmitry V. Skryabin. Bistable Topological Insulator with Exciton-Polaritons. *Physical Review Letters*, 119(25):253904, 2017.
- [134] Roger S. K. Mong and Vasudha Shivamoggi. Edge states and the bulk-boundary correspondence in Dirac Hamiltonians. *Physical Review B*, 83(12):125109, March 2011. Publisher: American Physical Society.
- [135] S. Longhi. Probing one-dimensional topological phases in waveguide lattices with broken chiral symmetry. *Opt. Lett.*, 43(19):4639, October 2018.
- [136] Bo-Hung Chen and Dah-Wei Chiou. An elementary rigorous proof of bulk-boundary correspondence in the generalized Su-Schrieffer-Heeger model. *Physics Letters A*, 384(7):126168, March 2020.
- [137] Natalia Malkova, Ivan Hromada, Xiaosheng Wang, Garnett Bryant, and Zhigang Chen. Observation of optical Shockley-like surface states in photonic superlattices. *Optics Letters*, 34(11):1633, June 2009. Publisher: Optical Society of America.
- [138] Marcos Atala, Monika Aidelsburger, Julio T. Barreiro, Dmitry Abanin, Takuya Kitagawa, Eugene Demler, and Immanuel Bloch. Direct measurement of the Zak phase in topological Bloch bands. *Nature Physics*, 9(12):795–800, November 2013. Publisher: Nature Research.
- [139] Eric J. Meier, Fangzhao Alex An, and Bryce Gadway. Observation of the topological soliton state in the Su–Schrieffer–Heeger model. *Nature Communications*, 7:13986, December 2016. Publisher: Nature Publishing Group.
- [140] Sergey Kruk, Alexey Slobozhanyuk, Denitza Denkova, Alexander Poddubny, Ivan Kravchenko, Andrey Miroshnichenko, Dragomir Neshev, and Yuri Kivshar. Edge States and Topological Phase Transitions in Chains of Dielectric Nanoparticles. *Small*, 13(11):1603190, January 2017.
- [141] Andrea Blanco-Redondo, Imanol Andonegui, Matthew J. Collins, Gal Harari, Yaakov Lumer, Mikael C. Rechtsman, Benjamin J. Eggleton, and Mordechai Segev. Topological Optical Waveguiding in Silicon and the Transition between Topological and Trivial Defect States. *Physical Review Letters*, 116(16):163901, April 2016. Publisher: American Physical Society.
- [142] D. D. Solnyshkov, A. V. Nalitov, and G. Malpuech. Kibble-Zurek Mechanism in Topologically Nontrivial Zigzag Chains of Polariton Micropillars. *Physical Review Letters*, 116(4):046402, January 2016. Publisher: American Physical Society.

- [143] C. E. Whittaker, E. Cancellieri, P. M. Walker, B. Royall, L. E. Tapia Rodriguez, E. Clarke, D. M. Whittaker, H. Schomerus, M. S. Skolnick, and D. N. Krizhanovskii. Effect of photonic spin-orbit coupling on the topological edge modes of a Su-Schrieffer-Heeger chain. *Physical Review B*, 99(8):81402, February 2019. arXiv: 1812.02034 Publisher: American Physical Society.
- [144] Tristan H. Harder, Meng Sun, Oleg A. Egorov, Ihor Vakulchyk, Johannes Beierlein, Philipp Gagel, Monika Emmerling, Christian Schneider, Ulf Peschel, Ivan G. Savenko, Sebastian Klemmt, and Sven Höfling. Coherent Topological Polariton Laser. *ACS Photonics*, 8(5):1377–1384, May 2021.
- [145] Marco Dusel, Simon Betzold, Tristan H. Harder, Monika Emmerling, Johannes Beierlein, Jürgen Ohmer, Utz Fischer, Ronny Thomale, Christian Schneider, Sven Höfling, and Sebastian Klemmt. Room-Temperature Topological Polariton Laser in an Organic Lattice. *Nano Lett.*, 21(15):6398–6405, August 2021.
- [146] Ian Mondragon-Shem, Taylor L Hughes, Juntao Song, and Emil Prodan. Topological Criticality in the Chiral-Symmetric AIII Class at Strong Disorder. *Phys. Rev. Lett.*, 113(4):46802, 2014. Publisher: American Physical Society.
- [147] Maria Maffei, Alexandre Dauphin, Filippo Cardano, Maciej Lewenstein, and Pietro Massignan. Topological characterization of chiral models through their long time dynamics. *New J. Phys.*, 20(1):013023, January 2018.
- [148] Wange Song, Wenzhao Sun, Chen Chen, Qinghai Song, Shumin Xiao, Shining Zhu, and Tao Li. Breakup and Recovery of Topological Zero Modes in Finite Non-Hermitian Optical Lattices. *Physical Review Letters*, 123(16):165701, October 2019. Publisher: American Physical Society.
- [149] Midya Parto, Steffen Wittek, Hossein Hodaei, Gal Harari, Miguel A Bandres, Jinhan Ren, Mikael C Rechtsman, Mordechai Segev, Demetrios N Christodoulides, and Mercedeh Khajavikhan. Edge-Mode Lasing in 1D Topological Active Arrays. *Physical Review Letters*, 120(11):113901, March 2018. Publisher: American Physical Society.
- [150] Han Zhao, Pei Miao, Mohammad H Teimourpour, Simon Malzard, Ramy El-Ganainy, Henning Schomerus, and Liang Feng. Topological hybrid silicon microlasers. *Nature Communications*, 9(1):981, 2018.
- [151] D. Tanese, E. Gurevich, F. Baboux, T. Jacqmin, A. Lemaître, E. Galopin, I. Sagnes, A. Amo, J. Bloch, and E. Akkermans. Fractal Energy Spectrum of a Polariton Gas in a Fibonacci Quasiperiodic Potential. *Physical Review Letters*, 112(14):146404, April 2014.
- [152] Florent Baboux, Eli Levy, Aristide Lemaître, Carmen Gómez, Elisabeth Galopin, Luc Le Gratiet, Isabelle Sagnes, Alberto Amo, Jacqueline Bloch, and Eric Akkermans. Measuring topological invariants from generalized edge states in polaritonic quasicrystals. *Physical Review B*, 95(16):161114, April 2017. arXiv: 1607.03813 Publisher: American Physical Society.
- [153] Barry Bradlyn, L. Elcoro, Jennifer Cano, M. G. Vergniory, Zhijun Wang, C. Felser, M. I. Aroyo, and B. Andrei Bernevig. Topological quantum chemistry. *Nature*, 457:298–305, 2017.

- [154] J Cayssol and J N Fuchs. Topological and geometrical aspects of band theory. *J. Phys. Mater.*, 4(3):034007, July 2021.
- [155] M Blanco de Paz, M A J Herrera, P Arroyo Huidobro, H Alaeian, M G Vergniory, B Bradlyn, G Giedke, A García-Etxarri, and D Bercioux. Energy density as a probe of band representations in photonic crystals. *J. Phys.: Condens. Matter*, 34(31):314002, August 2022.
- [156] Nicolas Pernet, Philippe St-Jean, Dmitry D. Solnyshkov, Guillaume Malpuech, Nicola Carlon Zambon, Quentin Fontaine, Bastian Real, Omar Jamadi, Aristide Lemaître, Martina Morassi, Luc Le Gratiet, Téo Baptiste, Abdelmounaim Harouri, Isabelle Sagnes, Alberto Amo, Sylvain Ravets, and Jacqueline Bloch. Gap solitons in a one-dimensional driven-dissipative topological lattice. *Nat. Phys.*, May 2022.
- [157] María Blanco de Paz, Maia G. Vergniory, Dario Bercioux, Aitzol García-Etxarri, and Barry Bradlyn. Engineering fragile topology in photonic crystals: Topological quantum chemistry of light. *Phys. Rev. Research*, 1(3):032005, October 2019.
- [158] Long-Hua Wu and Xiao Hu. Scheme for Achieving a Topological Photonic Crystal by Using Dielectric Material. *Physical Review Letters*, 114(22):223901, June 2015.
- [159] Nikhil Parappurath, Filippo Alpeggiani, L Kuipers, and Ewold Verhagen. Direct observation of topological edge states in silicon photonic crystals: Spin, dispersion, and chiral routing. *Science Advances*, 6(10):eaaw4137, March 2020.
- [160] Mahmoud Jalali Mehrabad, Andrew P. Foster, René Dost, Edmund Clarke, Pallavi K. Patil, A. Mark Fox, Maurice S. Skolnick, and Luke R. Wilson. Chiral topological photonics with an embedded quantum emitter. *Optica*, 7(12):1690, December 2020.
- [161] A H Castro Neto, F Guinea, N M R Peres, K S Novoselov, and A K Geim. The electronic properties of graphene. *Rev. Mod. Phys.*, 81(1):109–162, 2009.
- [162] Kenichiro Kusudo, Na Young Kim, Andreas Löffler, Sven Höfling, Alfred Forchel, and Yoshihisa Yamamoto. Stochastic formation of polariton condensates in two degenerate orbital states. *Physical Review B*, 87(21):214503, June 2013.
- [163] M. Milićević, T. Ozawa, G. Montambaux, I. Carusotto, E. Galopin, A. Lemaître, L. Le Gratiet, I. Sagnes, J. Bloch, and A. Amo. Orbital Edge States in a Photonic Honeycomb Lattice. *Physical Review Letters*, 118(10):107403, March 2017. Publisher: American Physical Society.
- [164] B. Real, O. Jamadi, M. Milićević, N. Pernet, P. St-Jean, T. Ozawa, G. Montambaux, I. Sagnes, A. Lemaître, L. Le Gratiet, A. Harouri, S. Ravets, J. Bloch, and A. Amo. Semi-Dirac Transport and Anisotropic Localization in Polariton Honeycomb Lattices. *Phys. Rev. Lett.*, 125(18):186601, October 2020.
- [165] Kyoko Nakada, Mitsutaka Fujita, Gene Dresselhaus, and Mildred Dresselhaus. Edge state in graphene ribbons: Nanometer size effect and edge shape dependence. *Physical Review B*, 54(24):17954–17961, December 1996.
- [166] Mahito Kohmoto and Yasumasa Hasegawa. Zero modes and edge states of the honeycomb lattice. *Physical Review B*, 76(20):205402, November 2007.

- [167] M Milićević, T Ozawa, P Andreakou, I Carusotto, T Jacqmin, E Galopin, A Lemaître, L Le Gratiet, I Sagnes, J Bloch, and A Amo. Edge states in polariton honeycomb lattices. *2D Materials*, 2(3):034012, August 2015.
- [168] Mikael C. Rechtsman, Yonatan Plotnik, Julia M. Zeuner, Daohong Song, Zhigang Chen, Alexander Szameit, and Mordechai Segev. Topological Creation and Destruction of Edge States in Photonic Graphene. *Physical Review Letters*, 111(10):103901, September 2013.
- [169] Matthieu Bellec, Ulrich Kuhl, Gilles Montambaux, and Fabrice Mortessagne. Manipulation of edge states in microwave artificial graphene. *New Journal of Physics*, 16(11):113023, November 2014.
- [170] Congjun Wu, Doron Bergman, Leon Balents, and S. Das Sarma. Flat Bands and Wigner Crystallization in the Honeycomb Optical Lattice. *Physical Review Letters*, 99(7):070401, August 2007. Publisher: American Physical Society.
- [171] C. L. Kane and T. C. Lubensky. Topological boundary modes in isostatic lattices. *Nature Physics*, 10(1):39–45, December 2013. Publisher: Nature Publishing Group.
- [172] N Levy, S A Burke, K L Meaker, M Panlasigui, A Zettl, F Guinea, A H Castro Neto, and M F Crommie. Strain-Induced Pseudo-Magnetic Fields Greater Than 300 Tesla in Graphene Nanobubbles. *Science*, 329(5991):544 – 547, July 2010.
- [173] Jimin Kim, Seung Su Baik, Sae Hee Ryu, Yeongsup Sohn, Soohyung Park, Byeong-Gyu Park, Jonathan Denlinger, Yeonjin Yi, Hyoung Joon Choi, and Keun Su Kim. Observation of tunable band gap and anisotropic Dirac semimetal state in black phosphorus. *Science (New York, N.Y.)*, 349(6249):723–726, August 2015.
- [174] Leticia Tarruell, Daniel Greif, Thomas Uehlinger, Gregor Jotzu, and Tilman Esslinger. Creating, moving and merging Dirac points with a Fermi gas in a tunable honeycomb lattice. *Nature*, 483(7389):302–305, 2012.
- [175] Kenjiro K. Gomes, Warren Mar, Wonhee Ko, Francisco Guinea, and Hari C. Manoharan. Designer Dirac fermions and topological phases in molecular graphene. *Nature*, 483(7389):306–310, March 2012.
- [176] Mikael C Rechtsman, Julia M Zeuner, Andreas Tunnermann, Stefan Nolte, Mordechai Segev, and Alexander Szameit. Strain-induced pseudomagnetic field and photonic Landau levels in dielectric structures. *Nature Phot.*, 7(2):153–158, 2013.
- [177] Matthieu Bellec, Ulrich Kuhl, Gilles Montambaux, and Fabrice Mortessagne. Topological Transition of Dirac Points in a Microwave Experiment. *Physical Review Letters*, 110(3):033902, January 2013.
- [178] Matthieu Bellec, Charles Poli, Ulrich Kuhl, Fabrice Mortessagne, and Henning Schomerus. Observation of supersymmetric pseudo-Landau levels in strained microwave graphene. *Light: Science and Applications*, 9(1):146, 2020.
- [179] Yasumasa Hasegawa, Rikio Konno, Hiroki Nakano, and Mahito Kohmoto. Zero modes of tight-binding electrons on the honeycomb lattice. *Physical Review B*, 74(3):033413, July 2006. Publisher: American Physical Society.

- [180] B Wunsch and F Guinea and F Sols. Dirac-point engineering and topological phase transitions in honeycomb optical lattices. *New Journal of Physics*, 10(10):103027, 2008.
- [181] G. Montambaux, F. Piéchon, J.-N. Fuchs, and M. Goerbig. Merging of Dirac points in a two-dimensional crystal. *Physical Review B*, 80(15):153412, October 2009.
- [182] M Milićević, G Montambaux, T Ozawa, O Jamadi, B Real, I Sagnes, A Lemaître, L Le Gratiet, A Harouri, J Bloch, and A Amo. Type-III and Tilted Dirac Cones Emerging from Flat Bands in Photonic Orbital Graphene. *Physical Review X*, 9(3):31010, July 2019. Publisher: American Physical Society.
- [183] G. E. Volovik and K. Zhang. Black hole and hawking radiation by type-II Weyl fermions. *JETP Letters*, 104(9):645–648, 2016.
- [184] Huaqing Huang, Kyung-Hwan Jin, and Feng Liu. Black-hole horizon in the Dirac semimetal  $\text{Zn}_2\text{In}_2\text{S}_5$ . *Physical Review B*, 98(12):121110, September 2018. Publisher: American Physical Society.
- [185] Shan Guan, Zhi-Ming Yu, Ying Liu, Gui-Bin Liu, Liang Dong, Yunhao Lu, Yugui Yao, and Shengyuan A. Yang. Artificial gravity field, astrophysical analogues, and topological phase transitions in strained topological semimetals. *npj Quant Mater*, 2(1):23, December 2017.
- [186] C. L. Kane and E. J. Mele. Size, Shape, and Low Energy Electronic Structure of Carbon Nanotubes. *Physical Review Letters*, 78(10):1932–1935, March 1997. Publisher: American Physical Society.
- [187] F. Guinea, M. I. Katsnelson, and A. K. Geim. Energy gaps and a zero-field quantum Hall effect in graphene by strain engineering. *Nature Physics*, 6(1):30–33, January 2010. Publisher: Nature Publishing Group.
- [188] Xinhua Wen, Chunyin Qiu, Yajuan Qi, Liping Ye, Manzhu Ke, Fan Zhang, and Zhengyou Liu. Acoustic Landau quantization and quantum-Hall-like edge states. *Nature Physics*, 15(4):352–356, 2019.
- [189] Grazia Salerno, Tomoki Ozawa, Hannah M Price, and Iacopo Carusotto. How to directly observe Landau levels in driven-dissipative strained honeycomb lattices. *2D Materials*, 2(3):034015, September 2015. Publisher: IOP Publishing.
- [190] Omar Jamadi, Elena Rozas, Grazia Salerno, Marijana Milićević, Tomoki Ozawa, Isabelle Sagnes, Aristide Lemaître, Luc Le Gratiet, Abdelmounaim Harouri, Iacopo Carusotto, Jacqueline Bloch, and Alberto Amo. Direct observation of photonic Landau levels and helical edge states in strained honeycomb lattices. *Light Sci. Appl.*, 9(1):144, 2020.
- [191] Grazia Salerno, Tomoki Ozawa, Hannah M Price, and Iacopo Carusotto. Propagating edge states in strained honeycomb lattices. *Physical Review B*, 95(24):245418, June 2017. Publisher: American Physical Society.
- [192] Marius Jürgensen, Seababrata Mukherjee, and Mikael C. Rechtsman. Quantized nonlinear Thouless pumping. *Nature*, 596(7870):63–67, August 2021.

- [193] Marijana Milićević, Olivier Bleu, Dmitry Solnyshkov, Isabelle Sagnes, Aristide Lemaître, Luc Le Gratiet, Abdelmounaim Harouri, Jacqueline Bloch, Guillaume Malpuech, and Alberto Amo. Lasing in optically induced gap states in photonic graphene. *SciPost Physics*, 5(6):64, December 2018. Publisher: SciPost Foundation.
- [194] J K Asbóth, B Tarasinski, and P Delplace. Chiral symmetry and bulk-boundary correspondence in periodically driven one-dimensional systems. *Physical Review B*, 90(12):125143, September 2014. Publisher: American Physical Society.
- [195] M Bellec, C Michel, H Zhang, S Tzortzakis, and P Delplace. Non-diffracting states in one-dimensional Floquet photonic topological insulators. *EPL*, 119(1):14003, 2017.
- [196] Frederik Nathan and Mark S Rudner. Topological singularities and the general classification of Floquet–Bloch systems. *New Journal of Physics*, 17(12):125014, 2015. Publisher: IOP Publishing.
- [197] Karen Wintersperger, Christoph Braun, F. Nur Ünal, André Eckardt, Marco Di Liberto, Nathan Goldman, Immanuel Bloch, and Monika Aidelsburger. Realization of an anomalous Floquet topological system with ultracold atoms. *Nat. Phys.*, 16(10):1058–1063, October 2020.
- [198] Christof Weitenberg and Juliette Simonet. Tailoring quantum gases by Floquet engineering. *Nat. Phys.*, 17(12):1342–1348, December 2021.
- [199] Sebastian Geier, Nithiwadee Thaicharoen, Clément Hainaut, Titus Franz, Andre Salzinger, Annika Tebben, David Grimshandl, Gerhard Zürn, and Matthias Weidemüller. Floquet Hamiltonian engineering of an isolated many-body spin system. *Science*, 374(6571):1149–1152, November 2021.
- [200] Alois Regensburger, Christoph Bersch, Benjamin Hinrichs, Georgy Onishchukov, Andreas Schreiber, Christine Silberhorn, and Ulf Peschel. Photon Propagation in a Discrete Fiber Network: An Interplay of Coherence and Losses. *Physical Review Letters*, 107(23):233902, December 2011. Publisher: American Physical Society.
- [201] Alois Regensburger, Christoph Bersch, Mohammad-Ali Miri, Georgy Onishchukov, Demetrios N Christodoulides, and Ulf Peschel. Parity–time synthetic photonic lattices. *Nature*, 488(7410):167–171, 2012.
- [202] Martin Wimmer, Mohammed-Ali Miri, Demetrios Christodoulides, and Ulf Peschel. Observation of Bloch oscillations in complex PT-symmetric photonic lattices. *Scientific Reports*, 5:17760, December 2015. Publisher: The Author(s).
- [203] Martin Wimmer, Monika Monika, Iacopo Carusotto, Ulf Peschel, and Hannah M. Price. Superfluidity of Light and Its Breakdown in Optical Mesh Lattices. *Phys. Rev. Lett.*, 127(16):163901, October 2021.
- [204] Martin Wimmer, Alois Regensburger, Mohammad-Ali Miri, Christoph Bersch, Demetrios N Christodoulides, and Ulf Peschel. Observation of optical solitons in PT-symmetric lattices. *Nature Communications*, 6(1):7782, 2015.

- [205] Albert F. Adiyatullin, Lavi K. Upreti, Corentin Lechevalier, Clement Evain, Francois Copie, Pierre Suret, Stephane Randoux, Pierre Delplace, and Alberto Amo. Multi-topological Floquet metals in a photonic lattice. *arXiv:2203.01056*, March 2022.
- [206] Corentin Lechevalier, Clément Evain, Pierre Suret, François Copie, Alberto Amo, and Stéphane Randoux. Single-shot measurement of the photonic band structure in a fiber-based Floquet-Bloch lattice. *Commun Phys*, 4(1):243, December 2021.
- [207] Lavi K Upreti, C Evain, S Randoux, P Suret, A Amo, and P Delplace. Topological Swing of Bloch Oscillations in Quantum Walks. *Physical Review Letters*, 125(18):186804, October 2020. Publisher: American Physical Society.
- [208] Xuzhe Ying and Alex Kamenev. Symmetry-Protected Topological Metals. *Phys. Rev. Lett.*, 121(8):086810, August 2018.
- [209] Longwen Zhou, Chong Chen, and Jiangbin Gong. Floquet semimetal with Floquet-band holonomy. *Physical Review B*, 94(7):75443, August 2016. Publisher: American Physical Society.
- [210] Hannah Price, Yidong Chong, Alexander Khanikaev, Henning Schomerus, Lukas J Maczewsky, Mark Kremer, Matthias Heinrich, Alexander Szameit, Oded Zilberberg, Yihao Yang, Baile Zhang, Andrea Alù, Ronny Thomale, Iacopo Carusotto, Philippe St-Jean, Alberto Amo, Avik Dutt, Luqi Yuan, Shanhui Fan, Xuefan Yin, Chao Peng, Tomoki Ozawa, and Andrea Blanco-Redondo. Roadmap on topological photonics. *J. Phys. Photonics*, 4(3):032501, July 2022.
- [211] S. R. K. Rodriguez, W. Casteels, F. Storme, N. Carlon Zambon, I. Sagnes, L. Le Gratiet, E. Galopin, A. Lemaître, A. Amo, C. Ciuti, and J. Bloch. Probing a Dissipative Phase Transition via Dynamical Optical Hysteresis. *Physical Review Letters*, 118(24):247402, June 2017. Publisher: American Physical Society.
- [212] S. R. K. Rodriguez, A. Amo, I. Sagnes, L. Le Gratiet, E. Galopin, A. Lemaître, and J. Bloch. Interaction-induced hopping phase in driven-dissipative coupled photonic microcavities. *Nature Communications*, 7:11887, June 2016. Publisher: Nature Publishing Group.
- [213] S. Rahimzadeh Kalaleh Rodriguez, A. Amo, I. Carusotto, I. Sagnes, L. Le Gratiet, E. Galopin, A. Lemaître, and J. Bloch. Nonlinear Polariton Localization in Strongly Coupled Driven-Dissipative Microcavities. *ACS Photonics*, 5(1), 2018.
- [214] N Carlon Zambon, S R K Rodriguez, A Lemaître, A Harouri, L Le Gratiet, I Sagnes, P St-Jean, S Ravets, A Amo, and J Bloch. Parametric instability in coupled nonlinear microcavities. *Physical Review A*, 102(2):23526, August 2020. Publisher: American Physical Society.
- [215] O. Jamadi, B. Real, K. Sawicki, C. Hainaut, A. González-Tudela, N. Pernet, I. Sagnes, M. Morassi, A. Lemaître, L. Le Gratiet, A. Harouri, S. Ravets, J. Bloch, and A. Amo. Reconfigurable photon localization by coherent drive and dissipation in photonic lattices. *Optica*, 9(7):706, July 2022.

- 
- [216] V. Goblot, H. S. Nguyen, I. Carusotto, E. Galopin, A. Lemaître, I. Sagnes, A. Amo, and J. Bloch. Phase-Controlled Bistability of a Dark Soliton Train in a Polariton Fluid. *Physical Review Letters*, 117(21):217401, November 2016. Publisher: American Physical Society.

